Theoretical studies of 2,4-DNT molecular structure and its interaction with siloxane surface of clays

THEORETICAL STUDIES OF 2,4-DNT MOLECULAR STRUCTURE AND ITS INTERACTION WITH THE SILOXANE SURFACE OF CLAYS

By

Carmen M. Ramos Reyes

A thesis submitted in partial fulfillment of the requirements for the degree of

MASTER OF SCIENCES
in
CHEMISTRY

UNIVERSITY OF PUERTO RICO
MAYAGÜEZ CAMPUS
2005

Approved by:

_____	_____
Samuel P. Hernández-Rivera, Ph.D. Member, Graduate Committee	Date
_____	_____
Miguel A. Muñoz, Ph.D. Member, Graduate Committee	Date
_____	_____
Nairmen Mina, Ph.D. President, Graduate Committee	Date
_____	_____
Satya Mandavilli, Ph.D. Representative of Graduate Studies	Date
_____	_____
María A. Aponte, Ph.D. Chairperson of the Department	Date

ABSTRACT

Among the many different signature compounds emitted from a landmine in the vapor phase, 2,4-DNT is the most common nitroaromatic compound used to detect buried landmines. This study presents ab initio quantum mechanical calculations on the interaction of 2,4-DNT (DNT) with the basal siloxane surface of the clay mineral kaolinite. Theoretical calculations of the low energy conformation of DNT interacting with the siloxane surface of clay minerals were performed to determine obtain their properties once adsorbed as well as the structure of the adsorbed molecule. The calculations also indicate the orientation of DNT adsorbed on the clay surface and the effect of adsorption. This study was performed using DFT, DFT//HF and MP2//HF methods taking into account the contribution of the Coulombic (CE_b) and dispersion (DE_b) energies, to obtain the binding energies between DNT and siloxane surface. A comparison of the CE_b and DE_b energies shows that the stabilization of DNT at the siloxane sites is mainly provided by dispersion interaction energy. Considering the accuracy and cost of the computation methods the 6-31+G* basis set produced the best representation of the interaction energy (42 kJ/mol) using the MP2//HF level of theory for the interaction. These theoretical calculations give a good prediction of the interaction between the 2,4-DNT molecule with soil clay minerals. The computational results are compared with the experimental results obtained with the FT-IR microspectroscopic technique. A solvation analysis, using water as solvent, was performed to the DNT, the PCM solvation model affects significantly the spectroscopic signature of the explosive molecule.

RESUMEN

Entre los diversos compuestos en fase gaseosa emitidos de una mina terrestre, el 2,4-DNT es uno de los compuestos nitroaromáticos más comunes, y es utilizado en términos de detectar estas minas enterradas. Este estudio presenta cálculos mecánicos cuánticos ab initio de la interacción del DNT con la superficie basal, de siloxano, del mineral arcilloso caolinita. Se efectuaron cálculos teóricos del confórmero más estable del DNT interactuando con la superficie de siloxano del mineral arcilloso para obtener sus propiedades una vez es absorbido, así como la estructura de la molécula absorbida. Además, los cálculos recrean la forma en que se orienta el DNT y los efectos de la adsorción de éste a la arcilla. Este estudio fue realizado usando los métodos de DFT, DFT//HF y MP2//HF tomando en cuenta la contribución de la energía Coulómbica (CE_b) y de la energía de dispersión (DE_b), para obtener la energía de enlace entre el DNT y la superficie de siloxano. La comparación entre las energías CE_b y DE_b muestra que la estabilización del DNT en el siloxano es provista principalmente por la energía de dispersión. Considerando la exactitud y el costo computacional de los métodos, el basis set 6-31+G* es el que produce la mejor representación de la energía de interacción (42 kJ/mol) usando el nivel de teoría MP2//HF para la interacción. Los resultados computacionales son comparados con resultados experimentales obtenidos con la técnica de microespectroscopía infrarroja (FT-IR). Se realizó un análisis en el que se percibió el efecto de solvatación, usando agua como solvente, en la molécula de DNT, siendo el modelo de solvatación PCM el que produjo cambios significativos en la firma espectroscópica del explosivo.

ACKNOWLEDGMENTS

I want to thank God who gave me the wisdom and knowledge to carry out this work, which was accomplished with a lot of effort.

Thanks to my parents, my brother and my sister because, every time that I visited or called them, they brought me support, encouragement and strength to go on with my carrier. Mom and Dad these years far from you were not in vain!!

Of course I have to thanks my laboratory partners Liliana, Neiza, Rosangela and Yleana, the Mina's girls, for making these years ones much more tolerable, despite all the hard work. Thanks for the comradeship that existed in our working environment. Although with different personalities, we have in common the respect and the affection for each another.

This research could not be possible without an excellent guide, like that offered by my chairman, Dr. Nairmen Mina. Thanks professor for allowing me to be part of your working team and for trusting me.

Another person that contributed to the development of this work was Dr. Alberto Santana...thank you so much.

I am grateful of the economical support from the U.S. Department of Defense (DoD) MURI Program under grant No DAAD 19-02-1-0257 and from the Center for Chemical Sensor Development for Explosives (CCSDE).

LIST OF CONTENTS

LIST OF TABLES

LIST OF FIGURES

APPENDIX

I. INTRODUCTION

Nitroaromatic compounds (NAC's) comprise an important class of potential environmental contaminants[1] because of their wide use as agrochemicals, textile dyes, munitions and other classes of industrial chemicals[2,3]. As a result, there has been considerable interest in determining the fate and pathways of NAC's in soil and aquatic environments. The manufacturing of 2,4,6-trinitrotoluene (TNT), a NAC and the most common explosive in landmines, has as a byproducts dinitrotoluene (DNT) isomers. DNT can be found in buried landmines representing not only an environmental threat but also risk for humanity.

Detection of buried landmines relies mainly on the detection of the chemical signatures emanating from the soil. 2,4-DNT, which is a manufacturing impurity of military-grade TNT, have an equilibrium vapor concentration higher than that of TNT by at least one order of magnitude. This fact makes the concentration of 2,4-DNT in the chemical vapor signature of a landmine higher than that of trinitrotoluene. DNT has been detected in the soil, surface water, and groundwater near by sites that contains buried munitions wastes[4]. Since soils usually have large surface areas; the probability for DNT sorption onto soil particles is vast. We are interested in the types of interactions responsible for the adsorption of DNT to soil surfaces. In order to obtain a representation of the different types of surface sites in the soil environment, we choose the siloxane surface of the homoionic clay mineral kaolinite as the model for the adsorption process.

Nitroaromatic chemicals have very little vapor pressure making the detection of their chemical signature very difficult. Thus, selecting the appropriate technology for their detection and to identify buried landmines is not an easy task. The detection of trace level of explosives is of great importance to national security, and very useful for landmine detection, military branches, and many civil engineering operations. In addition, soil contamination with toxic explosives at military bases is a major environmental problem. Established and emerging technologies focus on decreasing the limits of detection and increasing the selectivity toward discriminating among the various types of explosives.

Recently, efforts have been focused on the understanding of transport processes that allow the explosive chemicals to move from the landmine to the surroundings[5]. Buried landmines release signature compounds to the environment. They are released into the surroundings from surface contamination of the cases or vapor phase diffusion, and by leakage through cracks, seams, and holes in the mine. Eventually, a fraction of these compounds, which are the landmine signature, reaches the surface and escape to the environment where they can be detected by chemical sensing explosive methods such as vapor sniffers, two photon-fluorescence spectroscopy, infrared and Raman imagining, API-TOF-MS, TEA-GC, IMS, GPR, canines, artificial sensors, and MEMS.

However, the transport mechanisms and fate of explosives molecules released from the landmine to the soil, ground, water, and air is a very complex process and depends on many factors such as temperature, type of soil, season, rainfall, wind, and sunlight intensity and duration, among others. In addition, when particles or vapor escape of the explosive from the landmine they may interact with the surfaces that they encounter in their way out. These explosive-surface interactions can be chemical or physical depending on the type of materials. These types of interactions could lead to adsorption of the explosives chemicals to the soil components (e.g. polymers, metals, salts, organic matter etc).

Microbial degradation can also play an important role by transforming the organic compounds present in the soil[6]. Once the chemicals are outside the landmine container they can also be partitioned into the soil-air, soil-water and even undergo phase transitions. All these processes are affected by temperature, humidity, evaporation, precipitation, organic matter, and type of minerals present in the soil. In order to determine that chemical signature it is necessary to understand the possible ways and types of interactions, at the molecular level. In this regard, quantum mechanical calculations, which have proven very helpful in increasing our understanding of molecular level interaction processes, could play a major role in the study of the DNT-soil interactions. In a quantum mechanical study of the interaction of dinitrotoluenes with soil clay mineral surfaces, the calculated interaction energy can be related to the thermodynamic adsorption function.

We have subjected the 2,4-DNT explosive, to both ab initio treatments and density functional theory (DFT) level of theory. Gaussian 03 package program[7] was used in this study in order to investigate the most stable conformations of 2,4-DNT. Their symmetry and vibrational spectra were also determined. In addition, the binding energy of DNT with the siloxane site surface of the clay mineral kaolinite was calculated. These calculations will allow us to determine the types as well as the modes of interactions of 2,4 DNT with clay. The information will play a central role in determining the chemical spectroscopic signature of DNT in soil environments. The effects of the soil environment on the DNT chemical signature emanating from landmines, was analyzed using theoretical calculation and IR experimental techniques.

II. GENERAL OVERVIEW

II.1 2,4-Dinitrotoluene (DNT)

DNT is a pale yellow to brown-yellow crystalline solids at normal atmospheric temperature and is bitter, toxic, non-hygroscopic and combustible. It dissolves in water slightly but easily dissolves in organic solvents such as ether, acetone, benzene and toluene. It is a main raw material for synthesizing toluene-diisocyanate. DNT (Figure 2.1) has melting and boiling points at 71 ºC and 300 ºC, respectively. Its crystal density is 1.3208 g/cm^3 at 71 ºC[8]. Several isomers of DNT are manufacturing impurities in military-grade TNT and have been found to be present in most domestic and foreign TNT samples[9].

With respect to explosives-derived signatures, laboratory test indicated that equilibrium vapor concentrations of 2,4-DNT generally exceed by at least an order of magnitude for military-grade TNT's. Therefore, it could be useful to characterize a mine by detecting the vapor of one of those impurities. Other applications include uses as an intermediate in the manufacture of polyurethanes.

II.2 Kaolinite clay mineral

Soil is composed mainly of sand, silt and clay minerals and are divided in terms of their size; 2 mm - 0.05 mm, 0.05 mm - 2 μm and < 2 μm respectively[10]. Clay is the smallest soil component, therefore with higher surface area and a higher physical and chemical reactivity that indicate it is the responsible of the explosive

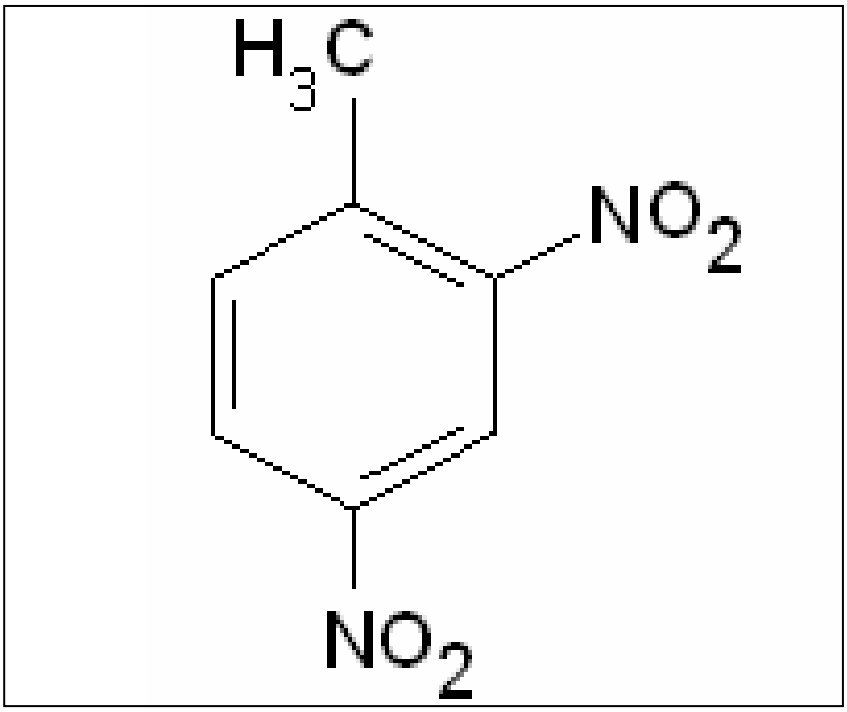

Figure 2.1 2,4- Dinitrotoluene (DNT) molecular structure

adsorption. The sand and silt chemical composition and structures are mainly inert.

The minerals are divided in classes that included: nitrates, sulfides, carbonates, sulfates, and silicates, among others. The silicate mineral class is an extremely large and important group of minerals. Nearly 40% of the common minerals are silicates and they constitute well over 90% of the Earth's crust and comprise the bulk of most soils[11]. The fundamental unit of all silicate structures is the SiO_4 tetrahedron. It consists of four O^{2-} ions at the apices of a regular tetrahedron coordinate to one Si^{4+} at the center. The individual tetrahedra are linked together by sharing O^{2-} ions to form more complex structures. According to the arrangement of the tetrahedra, they are classified as nesosilicates (single tetrahedra), cyclosilicates (rings), and phyllosilicates (sheets), among others. The clay fraction of most soils consists primarily of phyllosilicate minerals.

Phyllosilicate minerals strongly influence both the chemical and physical properties of soils because of their generally small particle sizes, high surface areas, and unique cation exchange properties. A clear understanding of the phyllosilicates minerals is central to understanding soil clay mineralogy and many environmental processes[12].

Kaolins are abundant in soils because they are not easily weathered, are formed in soils, and are frequently inherited from the soil parent material. As a result of these

characteristics, one of the kaolin minerals, kaolinite, is probably the most ubiquitous phyllosilicate clay mineral and is the most abundant phyllosilicate in highly weathered tropical soils. Only quartz is probable more common in soils than kaolinite. It lends its name to the kaolinite group members and also belongs to the larger general group known as clays. It is one of the most simple because can not be expanded[11].

Kaolinite, a 1:1 phyllosilicate structure (Figure 2.2), is composed of silicate sheets of Si_2O_5 bonded to aluminum oxide or hydroxide layers of $Al_2(OH)_4$, called siloxane and hydroxyl surfaces respectively. The siloxane and hydroxyl layers are tightly bonded together with weak bonding. The weak bonds between them cause the cleavage and softness of this mineral[13].

II.3 Computational chemistry methods

Computational chemistry is a technique that helps us to resolve, predict, and study new concepts, compounds, reactions and mechanisms. The technique is very useful with compounds that require extremely care in their handling, e.g. explosives, reducing risk to personnel testing and maintenance costs in service. Molecular modeling, a division of computational chemistry, focus on predict the behavior of individual molecules within a chemical system. Among the molecular characteristics that we can obtain with molecular modelling are:

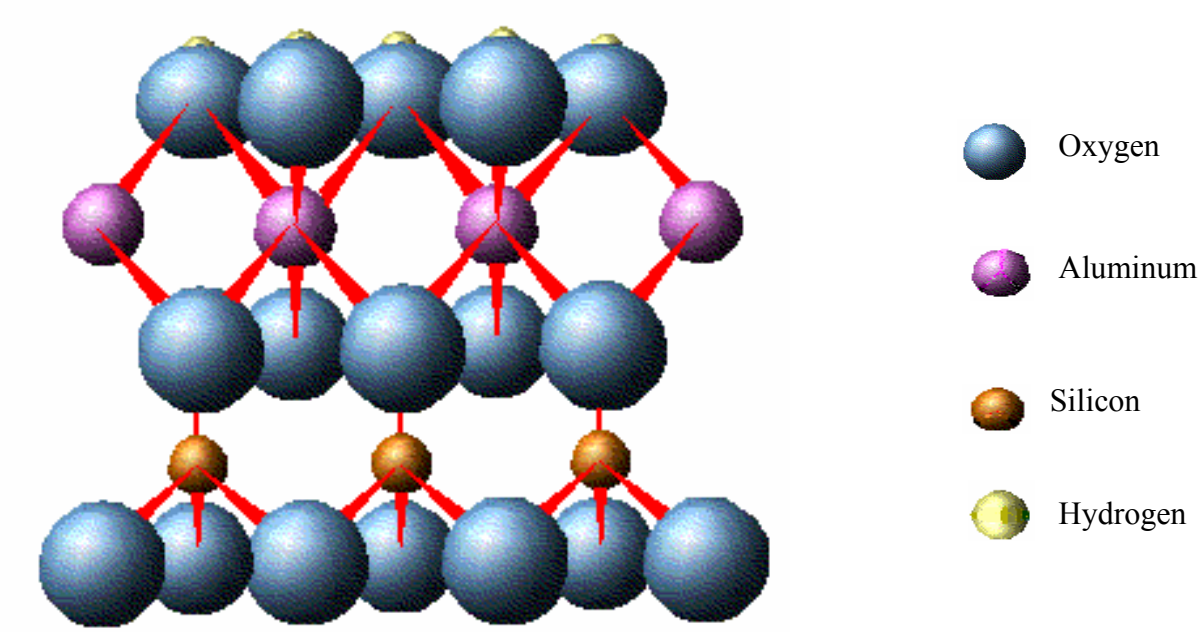

Figure 2.2 Molecular structure of Kaolinite.

- Heats of formation
- Bond and reaction energies
- Molecular energies and structure
- Energies and structures of transition states
- Charge distribution in molecules
- Vibrational frequencies (IR and Raman spectra)
- Electronic transitions

All molecular modeling techniques can be classified under three general categories: *ab initio* electronic structure calculations, semiempirical methods, and molecular mechanics. ***Ab initio*** or 'first principles' electronic structure methods are based upon quantum mechanics and therefore provide the most accurate and consistent predictions for chemical systems. This name is given to computations which are derived directly from theoretical principles, with no inclusion of experimental data. The approximations made are usually mathematical approximations, such as using a simpler functional form for a function or getting an approximate solution to a differential equation[15].

Semiempirical calculation methods are set up with the same general structure as a Hartree-Fock (HF) calculation. Within this framework, certain pieces of information, such as two electron integrals, are approximated or completely omitted. In order to correct for the errors introduced by omitting part of the calculation, the

method is parameterized, by curve fitting in a few parameters or numbers, in order to give the best possible agreement with experimental data.

The good side of this calculation method is that they are much faster than the ab initio calculations. The bad side of semiempirical calculations is that the results can be erratic. If the molecule being computed is similar to molecules in the data base used to parameterize the method, then the results may be very good. If the molecule being computed is significantly different from anything in the parameterization set, the answers may be very poor. Semiempirical calculations have been very successful in the description of organic chemistry, where there are only a few elements used extensively and the molecules are of moderate size. However, semi-empirical methods have been devised specifically for the description of inorganic chemistry[15].

If a molecule is too big to effectively use a semiempirical treatment, it is still possible to model its behavior by avoiding quantum mechanics totally. The methods referred to as **molecular mechanics** set up a simple algebraic expression for the total energy of a compound, with no necessity to compute a wave function or total electron density. The energy expression consists of simple classical equations, such as the harmonic oscillator equation in order to describe the energy associated with bond stretching, bending, rotation, and intermolecular forces, such as van der Waals interactions and hydrogen bonding. All of the constants in these equations must be obtained from experimental data or an ab initio calculation.

In a molecular mechanics method, the data base of compounds used to parameterize the method (a set of parameters and functions is called a force field) is crucial to its success. Semiempirical method may be parameterized against a set of organic molecules; whereas a molecular mechanics method may be parameterized against a specific class of molecules, such as proteins. Such a force field would only be expected to have any relevance to describing other proteins.

The good side of molecular mechanics is that it allows the modeling of enormous molecules, such as proteins and segments of DNA, making it the primary tool of computational biochemists. The bad side of molecular mechanics is that there are many chemical properties that are not even defined within the method, such as electronic excited states. In order to work with extremely large and complicated systems, often molecular mechanics software packages have the most powerful and easiest to use graphical interfaces. Because of this, mechanics is sometimes used because it is easy, but not necessarily a good way to describe a system[15].

II.3.1 Ab Initio Methods

For two-body systems, like the hydrogen atom, it is possible to solve the Schrödinger equation analytically. For systems with few electrons, such as helium, the "many-electron" problem can be solved more or less exactly (at present the non-relativistic ground state energy of helium is known with fifteen significant figures). More general many-electron systems cannot be treated with such precision, however.

A majority of the elements in the periodic table are many-electron systems where the motion of every electron is coupled to the motion of all the other electrons as well as to the nucleus. To study such systems we have to rely on some approximation methods.

The term ab initio means from first principles. It does not mean that we are solving the Schrödinger equation exactly. It means that we are selecting a method that in principle can lead to a reasonable approximation to the solution of the Schrödinger equation and then selecting a basis set that will implement that method in a reasonable way. By reasonable, we mean that the results are adequate for the application in hand. A method and basis set that is quite adequate for one application may be totally inadequate for another application. We also have to take into account the cost of doing calculations and the total amount of computer time required. The most popular ab initio methods that are: Hartree-Fock (HF), Moller-Plesset (MP) perturbation, couple-cluster (CC) and density functional theory (DFT) [16]. There are several differences in opinion about if DFT has to be considered purely ab initio or semi-empirical method. Each class contains diverse methods that use different theory variants, typically oriented to a concreted molecular property or to a special group of molecules. The proliferation of these methods shows that there is not an unique method adequate enough for all purposes.

II.3.1.1 Hartree-Fock (HF) method

Hartree-Fock method is one widely used approximation method. It is based on the rather natural approximation that every electron moves in the potential created by the nucleus plus the average potential of all the other electrons. This assumption leads to the independent-particle model, which essentially reduces the many-electron problem to the problem of solving a number of coupled single-electron equations. The single-electron equations are solved in an iterative manner until a chosen level of self-consistent accuracy is achieved. The Hartree-Fock approximation is a fast and reliable method for a wide range of atomic systems, but it is just a *first* approximation. There are several calculation schemes developed to generate improved results.

The primary approximation in the Hartree Fock method is called the central field approximation. This means that the Coulombic electron-electron repulsion (electron correlation) is not specifically taken into account. However, its net effect is included in the calculation. This is a variational calculation, meaning that the approximate energies calculated are all equal to or greater than the exact energy. The energies calculated are usually in units called Hartrees (1 H = 27.2114 eV). The energies are always greater than the exact energy and approach a limiting value called the Hartree Fock limit.

The "Hartree-Fock limit" has the best HF wave function and is reach with such a large and flexible basis set. The problem is that electrons are not paired up in the way that the Hartree-Fock method supposes. It suggests that the two electrons have

the same probability of being in the same region of space as being in separate symmetry equivalent regions of space. For example, in H_2 it would give the same probability of both electrons being near one atom as one being near one atom and the other near the second atom.

One of the limitations of HF calculations is that they do not include electron correlation. This means that HF takes into account the average affect of electron repulsion, but not the explicit electron-electron interaction. We call this effect "correlation". The difference in energy between the exact result and the Hartree-Fock limit energy is called the "correlation energy"[15]. Within HF theory the probability of finding an electron at some location around an atom is determined by the distance from the nucleus but not the distance to the other electrons. This is not physically true, but it is the consequence of the central field approximation, which defines the HF method. Any method which goes beyond HF in attempting to treat this phenomenon properly is known as an electron correlation method or a post-HF method[14].

II.3.1.2 Electron *correlation*

A number of types of calculations begin with HF calculation and then correct for correlation. Some of these methods are Moller-Plesset perturbation theory (MPn, where n is the order of correction), configuration interaction (CI), and coupled cluster theory (CC). Including correlation improves the accuracy of computed energies and

molecular geometries. For organic molecules, correlation is an extra correction for very-high accuracy work, but is not generally needed to obtain quantitative results[15].

II.3.1.2.a Moller-Plesset perturbation method

Correlation can be added as a perturbation from the Hartree-Fock wave function. This is called MP perturbation theory. In mapping the HF wave function onto a perturbation theory formulation, HF becomes a first-order perturbation. Thus, a minimal amount of correlation is added by using the second-order MP2 method. Moller-Plesset perturbation theory assumes that the effects of electron correlation are minor, and can be described by small corrections (perturbations) to the HF solution[15].

II.3.1.2.b Density Functional Theory (DFT)

The best DFT methods achieve significantly greater accuracy than Hartree-Fock theory at only a modest increase in computational cost (far less than MP2 for medium-size and larger molecular systems). They do so by including some of the effects of electron correlation with much less computational cost than traditional correlated methods. DFT methods compute electron correlation via general functionals of the electron density. Such methods are based on the Hohenberg-Kohn theorem, published in 1964, which demonstrated the existence of a unique functional which determines the exact ground state energy and density. The theorem does not provide the form of this functional, however.

Following on the work of Kohn and Sham, the approximate functionals employed by current DFT methods partition the electronic energy into several terms:

$$E = E^T + E^V + E^J + E^{XC} \quad (1)$$

where E^T is the kinetic energy term (arising from the motion of the electrons), E^V includes terms describing the potential energy of the nuclear-electron attraction and of the repulsion between pairs of nuclei, E^J is the electron-electron repulsion term (it is also described as the Coulomb self-interaction of the electron density), and E^{XC} is the exchange-correlation term and includes the remaining part of the electron-electron interactions[14]. The terms $E^T + E^V + E^J + E^{xc}$ represent the classical energy of the electron distribution, while E^{xc} represents both the quantum mechanical exchange energy, which accounts for electron spin, and the dynamic correlation energy due to the concerted motion of individual electrons.

Pure DFT methods calculate E^{xc} by pairing an exchange functional with a correlation functional and so are designated by the choice of combination. For example, BLYP combines Becke's gradient-corrected exchange functional with the gradient-corrected correlation functional of Lee, Yang and Parr[17].

II.3.1.3 Basis *Sets*

Basis sets are a variety of mathematical functions used to resolve a differential equation. In quantum chemical calculations, this term is applied to gaussian curves that represent atomic orbitals, which are optimized to reproduce the chemical

properties of a system. Basis sets vary in size and in their description of the electrons in different atomic orbitals. As long as the basis sets get larger they include more of basis functions which improve the calculations but involve a high computational cost. Also, it is possible adding polarize and diffuse functions. There are two general categories of basis sets[17].

II.3.1.3.a Minimal basis sets

A minimal basis set describes only the most basic aspects of the orbitals. The essential idea of the minimal basis set is that it selects one basis function for every atomic orbital that is required to describe the free atom. For example, the minimal basis set for the methane molecule consists of 4 1s orbitals, one per hydrogen atom, and the set of 1s, 2s and 2p that describes the carbon. The total basis set comprises 9 basis functions. All basis sets equations that use Slater Type Orbitals (STO) in the form STO-kG are considered to be "minimal" basis sets. STO are more exact, but take much longer to calculate than Gaussian Type Orbitals (GTOs) and you can get a good approximation of the STO adding several GTOs to the calculations. STO-kG means that you are modeling a STO calculation, with "k" number of GTOs[17].

II.3.1.3.b Split valence basis sets

In split valence basis sets, additional basis functions (one contracted gaussian plus some primitive gaussians) are allocated to each valence atomic orbital. The resultant linear combination allows the atomic orbitals to adjust independently for a

given molecular environment. Split valence basis sets are characterized by the number of functions assigned to valence orbitals.

Figure 2.3 shows a replace of each minimal basis set orbital by two orbitals. In each molecular orbital both orbitals of the set appear and they will mix in the ratio that gives the lowest energy. The combination of a large orbital and a small orbital is essentially equivalent to an orbital of intermediate size.

The resulting orbital is of a size that best fits the molecular environment since it is obtained from minimizing the energy. For example, consider the 6-31G* for H and C. For H, there is only one valence electron, and it is represented by two orbitals, one constructed of 3 primitives and the other with 1 primitive. With C, the s-orbital is a core orbital, and is represented by 6 gaussian primitives. The sp-orbital, on the other hand, is a valence orbital, and is represented by two orbitals, one with 3 gaussians and the other with 1.

It is also quite common to use split valence basis sets where the valence orbitals are split into say three, rather than two, functions. For example, let us consider

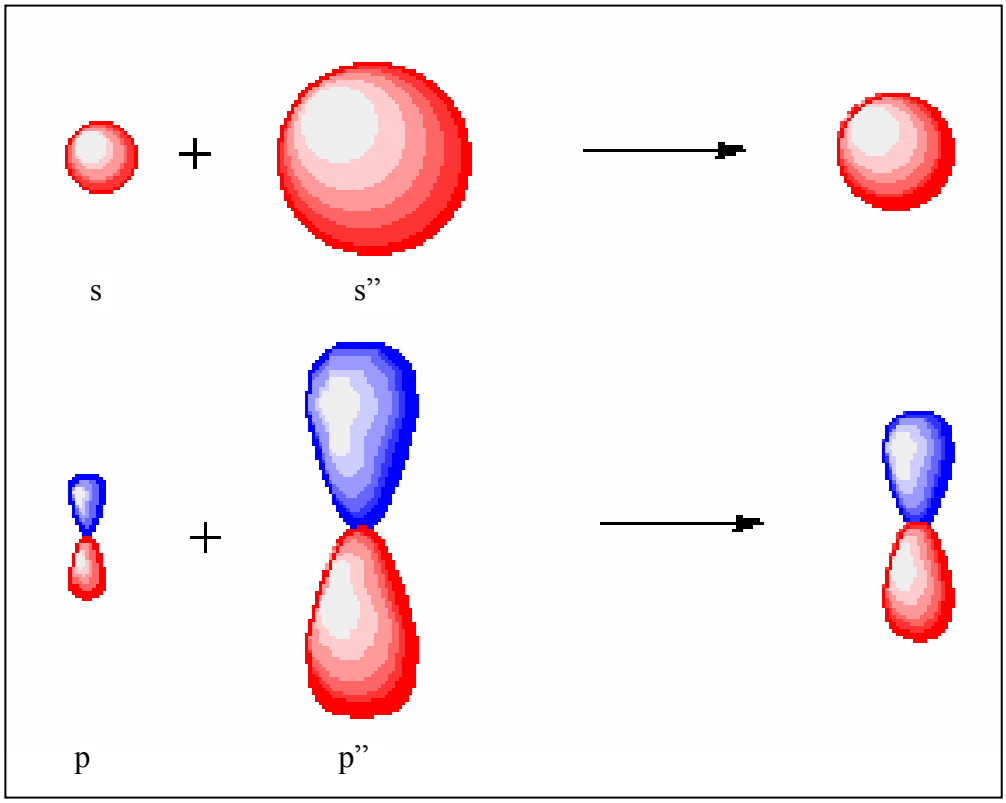

Figure 2.3 Effect of the split valence basis set

the 6-311G* basis set. The 6 represents the 6 gaussian primitives used to calculate the s-shell, the 3 represents the number of GTOs for one of the sp-shells and each 1 represents the number of GTOs for the other two sp-shells[18].

II.3.1.3.c Extended basis sets

Extended basis sets describe the orbitals in great detail. This basis set can have a variety of different polarisation functions and diffuse functions added. Non-uniform displacement of charge away from the atomic nuclei can be taken in account using the **polarization functions** in order to improve the chemical bonding description. For best approximation we have to take in mind that the orbitals share properties of "s" and "p" or of "p" and "d" orbitals. Therefore, they do not have individual orbital characteristics. As long as the atoms get close, their charge distribution cause a polarization effect, whose positive charge shift to one side and the negative charge move to the other side, producing the atomic orbitals distortion.

In Figure 2.4, we can see the effect of the polarization functions, in which the "s" orbitals are affected for the "p" orbitals and the "p" orbitals are affected for the "d" orbitals. The asterisk (*) is the symbol used to add the polarization functions to the basis sets. One * at the end of the basis set denote that "p" orbitals were polarized getting properties of "d" orbitals. The use of two ** indicate the polarization in "s" orbital with properties of "p" orbitals, in addition of "p" polarised orbitals.

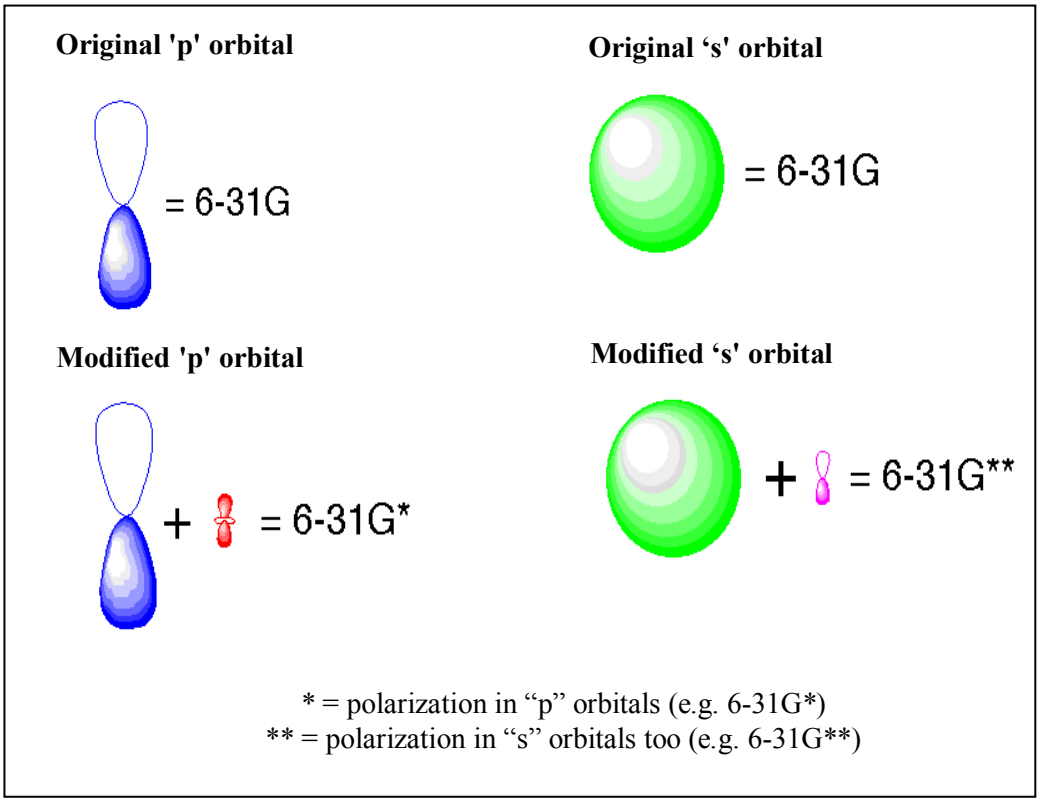

Figure 2.4 Effects of polarization functions added to the basis sets.

For the other side, **diffuse functions** are necessary to evaluate the species which significant electronic density was far of the nuclear center, so that the outermost weakly electrons have to be taken into account. The plus symbol (+) is used to add gaussian diffuse functions of s and p type to the basis sets. One + indicate that at all atoms, except H atoms, diffuse functions are included. Using two plus symbols (++), add these functions to all atoms including the H atoms[17].

II.3.2 Intermolecular interaction energy

The calculation of interaction energy is a very difficult task the interactions are normally very weak. These weak interaction energies are called noncovalent interactions because there is not breaking or formation of covalent bonds in the molecular complex formation process. Although the noncovalent interactions may be intra- or intermolecular, in this study we considerate the intermolecular interactions only because the intramolecular are too weak to affect the properties of the molecules in most cases. The noncovalent interaction is obtained calculating the binding energies (E_b) between the fragments of the complex.

Two main approaches exist in this field, the symmetry adapted perturbation theory (SAPT) approach[19,20], in which interaction energies are evaluated directly, and supermolecular approach, in which interaction energies are obtained as the difference between the total energies of the complex and its constituent parts. The SAPT approach has long suffered from the practical problem that the available programs

could evaluate only the simpler of the numerous energy contributions that arise in this theory. However, the newer programs are more complete, and accurate results for systems built from two fragments may be within reach.

The supermolecular approach has several practical as well as conceptual advantages over the SAPT approach[20]. Use is made of standard quantum chemical software, which employs highly efficient algorithms and which is widely available. The approach allows one to study both weakly and strongly interacting systems. The systems may contain any number of fragments and the effects of nonadditivity can be studied easily. In the supermolecular method, the interaction energy of a complex AB can be defined as the difference

$$\Delta E = E^{AB}(R) - E^{A} - E^{B} \qquad (2)$$

where R is the A-B distance, E^{AB} is the complex energy, E^{A} is the fragment A energy and E^{B} is the fragment B energy. In equation 2, E^{A} and E^{B} are assumed to be evaluated using the A basis set for E^{A} and the B basis set for E^{B}.

The interaction energy or binding energy is form as a contribution of these four different intermolecular energies:

$$E_{\text{int}} = E_{es} + E_{pol} + E_{dis} + E_{ex} \qquad (3)$$

where E_{es}, E_{pol}, E_{dis} and E_{ex}, represent electrostatic, polarization, dispersion, and exchange energy separately[21]. The intermolecular interaction was obtained calculating the binding energies between the fragments of the complex.

In the supermolecular method, all ab initio methods can be employed for intermolecular interaction calculation. However, not all of them are suitable for super molecular calculations. The HF method completely misses the dispersion interaction, which involves electron correlation between electrons on different molecules. In ab initio calculations, the total interaction energy can be divided into two parts: HF (ΔE_{HF}) and correlation energy (ΔE_{COR}):

$$\Delta E_{\text{int}} = \Delta E_{HF} + \Delta E_{COR} \tag{4}$$

ΔE_{COR} represents mainly the dispersion interaction energy. In post HF methods, the correlation term can be evaluated. The effective ones should give accurate values of ΔE_{COR}.

Density functional theory (DFT) is very attractive for intermolecular energy calculation because it is much less computationally demanding than post-HF methods. As the exchange-correlation functionals are naturally contained in DFT, it was believed that this method is suited to deal with intermolecular interactions. Disappointingly, current density-functional methods fail completely for the evaluation of dispersion energy due to the fact that none of the existing correlation functionals can describe the dispersion interaction[22,23]. The most economical post HF method is second-order Moller-Plesset theory (MP2). This is due to mutual compensation of neglected higher order contributions[24].

The main problem of this approach has been the Basis Set Superposition Error (BSSE) associate that can be deal by calculating the interaction energy with the counterpoise method.

II.3.3 Basis Set Superposition Error (BSSE)

Considering a chemical system AB composed of two interacting fragments A and B, the interaction energy between them can be expressed simply as the difference of the energy of the complex AB and the energy of its fragments A and B. Even though there are methods to compute directly the interaction energy by means of Intermolecular Perturbation Theory[19], this straightforward scheme, called supermolecular approximation, has been and nowadays still is the most common procedure for the quantitative determination of interaction energies.

The basis sets commonly used to calculate the interaction energy are far from being saturated and, hence, in any complex (gas phase or surface) each subsystem will tend to use the basis functions of the other subsystem improving their descriptions. This gives nonphysical, stabilizing contributions to the energy of the complex, and may also lead to artificial charge transfer if the basis set description of the subsystems is unbalanced. The energies obtained at the equilibrium geometry of the complex for each subsystem, are lower than the energies calculated at the same geometry with the basis functions of the respective subsystem alone.

Hence, there is an error of the interaction energy which is connected with the superposition of the orbitals of the subsystems. This effect was called Basis Set Superposition Error (BSSE) and was firstly pointed out by Jansen and Ros[25] in 1969, although the terminology BSSE was first introduced by Liu and McLean[26] in 1973.

The most convenient way of eliminate the BSSE would be the use of exact wave functions, thus avoiding the truncation of the basis set. The use of an infinite basis set is not feasible from a computational point of view but the basis sets of the interacting fragments could be improved in such a way that the presence of the basis functions of the partner would not further improve the description of the considered fragment.

On the other side, Boys and Bernardi, in 1970, proposed the use of a counterpoise (CP)[27] function in order to calculate the interaction energy of a given complex in such a way that the separate energies of the subsystems are calculated using the full set of basis functions used in the calculation of the energy of the complex. To the basis sets of each subsystem are added all basis functions of the other subsystem without its electrons and nuclei (ghost functions).

II.3.4 Solvation

Solvent is represented as a continuous dielectric without discrete internal structure and described only by its macroscopic dielectric constant. Solute is

embedded in a cavity of certain shape and size. The solute charge distribution interacts with the medium, polarizing it and creating a reflection charge distribution on the cavity surface (the reaction field) which, in turn, will interact electrostatically with the solute leading to the net stabilization.

II.3.4.1 PCM solvation model

The Polarizable Continuum Model (PCM) by Tomasi and coworkers is one of the most frequently used continuum solvation methods and has numerous variations over the years. This model assumes that the solvent is a continuum dielectric, which generates a reaction field interacting with the solute charge distribution. The cavity surface is defines as the sum of atomic spheres with radii taken as the atomic Van der Waals radii multiplied by a scaling factor of 1.2. PCM constitute a significant improvement in the description of solute-solvent interactions, provides us with a means of taking into account a mutual polarization of solute and solvent in a self-consistent way, and allows us to study molecules of complicated, non-spherical shape and charge distribution. In this case a cavity has a much more realistic shape and is constructed of certain number of interlocking spheres[28].

II.3.4.2 Onsager solvation model

The basic assumption made in the Onsager model is that the solute is placed in a spherical cavity inside the solvent. The solvent is described as a homogeneous,

polarizable medium of constant dielectric constant. The solute dipole moment induces a dipole moment of opposite direction in the surrounding medium. Polarization of the medium in turn polarizes the charge distribution in the solvent. Most systems under study are, of course, far from spherical, casting serious doubt on the usefulness of this approach. One much more practical approach consists of calculating the molecular volume as defines through the contour of constant electron density, equating this (non-spherical) molecular volume to the radius of an (ideally spherical) cavity, and adding a constant increment for the closest possible approach of solvent molecules. This indicates that the cavity radius is nothing else but a freely adjustable parameter that defines how the solvent reaction field is coupled to the molecular dipole moment. It can thus also be used to adjust the theoretically calculated solvent effect to known experiments[29].

III. PREVIOUS WORKS

Dinitrotoluenes are intermediates in the manufacture of TNT and are used as ingredients in mining explosives and in some smokeless powder. ***P.C. Chen and co-workers***[30] performed a theoretical analysis about the molecular structures of six dinitrotoluene isomers, that includes 2,3-dinitrotoluene, 2,4-dinitrotoluene, 2,5-dinitrotoluene, 2,6-dinitrotoluene, 3,4-dinitrotoluene and 3,5-dinitrotoluene. The geometrical conformation of the dinitrotoluene explosives molecules help to understand the thermal decomposition mechanisms.

They wanted to determine the thermal decomposition mechanisms and resultant products. These properties can affect the prediction of the feasibility of large-scale synthesis, long-term stability for storage purposes, the sensitivity to various stimuli, equally the performance of the explosives and the detonation velocity. Although X-ray or microwave spectroscopy techniques provide geometrical structure information, it is not complete. A full optimization of bond lengths, angles and torsional angles were performed by semi-empirical PM3 method and those results were used as an input file to performed another optimization but in this case using the HF/6-31G* method.

The energies of those conformers were calculated to determine which one is the most stable. The results indicate that 3,5-dinitrotoluene was the most stable isomer. Deformations of the phenyl ring, torsion angles of the nitro and methyl groups are

observed due the steric effects in addition to the inductive and resonance effects. This analysis shows the existence of intramolecular hydrogen bonds between the hydrogen and oxygen atoms of the methyl and nitro group, respectively.

Polynitroaromatic compounds used as explosives and herbicides have higher adsorption coefficients (K_d), than non aromatic nitro compounds. ***S. B. Haderlein and coworkers***[1] found that the adsorption of the nitroaromatic compounds to clays is associated by electron donor-acceptor (EDA) complex with the oxygens present at the external siloxane surface of the clay minerals. K_d values were evaluated for NACs, including 2,4-DNT, in different clays resulting in a grade of affinity that increases in the order kaolinite < illite < montmorillonite. They observed that the K_d values for the NACs are similar for the different types of clays. This implied that the relative tendency of the NACs to be adsorbed does not dependent on the mineral structures.

E. Balan and coworker's[31] studied the accuracy of the ab initio approach by calculating the IR spectrum of kaolinite [$Al_2Si_2O_5(OH)_4$] a widespread clay mineral. They analyzed the kaolinite because it is widely used as a model system to investigate adsorption processes and surface properties of clay minerals. Also, IR spectroscopy technique was used to investigate hydroxyl groups and hydrogen bonding patterns in kaolinite in order to compare it with the theoretical calculations.

KBr pellets were prepared using approximately 2 mg of sample with 300 mg of KBr and analyzed using a Nicolet Magna 560 FT-IR spectrometer in the 250-4000 cm^{-1} range with a resolution of 2 cm^{-1}. The theoretical calculations were performed by using the DFT and the generalized gradient approximation (GGA), which is based on the Becke, Lee, Yang and Parr (BLYP), to the exchange-correlation functional. Full-geometry optimization was accomplished in space group C_1 using a unit cell with 17 atoms.

Figure 3.1 shows the experimental and theoretical IR spectra of kaolinite. The experimental OH stretching bands are well defined at 3620, 3652, 3669 and 3695 cm^{-1}. The theoretical spectrum shows an excellent agreement with the experimental for wavenumbers higher than 500 cm^{-1}. The bands at 1008 and 1032 cm^{-1} can be unambiguously attributed to the anti-symmetric stretch of equatorial Si-O bonds. The bands at 1103 and 1112 cm^{-1} showed in the experimental spectrum correspond to the 1134 cm^{-1} band in the theoretical spectrum which is attributed to the in-phase stretch of apical Si-O bonds.

Therefore, they conclude that DFT calculations correctly reproduce the major features observed in experimental IR spectra, particularly the positions of high-frequency OH stretching bands.

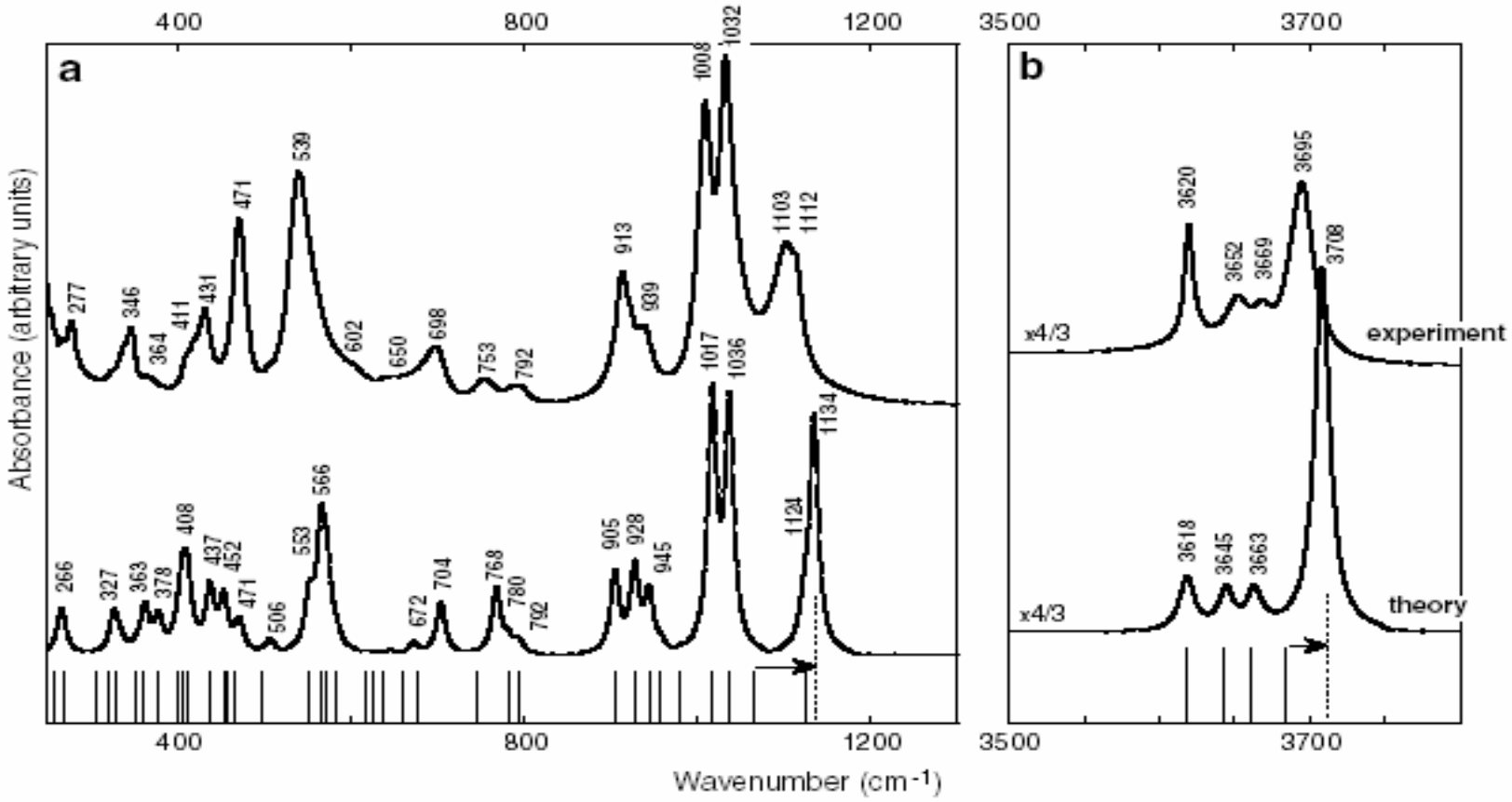

Figure 3.1 Experimental (top) and theoretical (bottom) IR absorption spectra of kaolinite: (a) mid-IR range, (b) OH-stretching region. Positions of the major features are indicated by their wavenumbers.

S. B. Haderlein and R. P. Schwarzenbach[32] studied the adsorption of a large number of nitroaromatic compounds (NACs) to mineral surfaces, particularly to homoionic kaolinites. The results demonstrate that NACs may adsorb specifically and reversibly to the negatively charged siloxane surface of kaolinite.

They compared the aluminum (hydr)oxides with the silica surfaces and found a somewhat larger affinity for 2,5-dinitrophenol (5-NO_2-2NP) and 1,4-dinitrobenzene (4-NO_2-NB) for two silica surfaces. The affinity of this compounds with the silica surfaces was of ~1 order of magnitude larger than the corresponding K_d value for the aluminum (hydr)oxides, but were still more than 3 orders of magnitude smaller than the K_d values for the Cs^+ -kaolinite.

They also studied the effect of branched alkyl substituent on the K_d value of a series of NACs and notice that substantially diminish the adsorption of the NAC even if they are not in the position ortho to the nitro group. These findings suggest that only NACs exhibiting a planar structure that allows the π-electron system to approach closely to the siloxane surface may strongly interact with the surface. The hypothesis that (particularly planar) NACs interact specifically with siloxane surface sites, at least if weakly hydrated cations are adsorbed, is corroborated by the large negative adsorption enthalpies (ΔH_{ads} = -40 ± 5 kJ/mol) found for several NACs for the adsorption on Cs^+ -kaolinite.

IV. MATERIALS & METHODS

IV.1 Materials

IV.1.1 Theoretical calculations analysis

- Gaussian 03 package of programs (GAUSSIAN, Inc., Pittsburgh, PA) were used to perform the calculations.
- Gauss View 3.0 was used to visualize the systems[33].
- Microwave workstation with dual processors and 4 Gb RAM.

IV.1.2 IR experimental analysis

- Reflection Fourier transformed infrared (FT-IR) microspectroscopy studies were performed using a Bruker Optics IFS 66 series FT-IR spectrometer coupled with Infrared Microscopy using a photovoltaic liquid N_2 cooled MCT detector equipped with the OPUS software 4.0.
- 2,4-DNT explosive standard solutions were obtained from Cerilliant Analytical Reference Materials, Austin, Texas. The DNT standard solution was certified as 1000 parts per million (ppm) and was dissolved successively with acetonitrile (ACN), in solutions of known concentration.
- The soil used for this study was obtained from the University of Puerto Rico Mayagüez campus.
- Pipettes (RAININ EDP3-Plus)
- Vortex to mix the interaction samples until they are homogeneous

- Centrifuge test microtubes
- Stainless steel surfaces
- Analytical balance (0.0001 g)

IV.2 Methods

IV.2.1 Theoretical Calculation Analysis

IV.2.1.1 Optimization of DNT

Theoretical calculations were performed with the Gaussian 03 package of programs. The Gauss View version 3.0 was used as visualization method. All quantum mechanical calculations were performed using the density functional theory (DFT) method with the hybrid B3LYP functional. This functional combines the Becke's three-parameter formula for exchange, i.e. B3, with the LYP gradient corrected correlation functional of Lee, Yang and Parr. This functional is a combination of Hartree-Fock self-interaction corrections with density functional exchange and corrections that take into account the Coulomb self interactions of the electrons.

The family of basis sets 3-21G, 6-31G, 6-311G, 6-311G(d) and 6-311+G (d,p) were used to get a full optimization of 2,4-DNT molecule with a C_1 symmetry. The gas-phase geometry was fully optimized without any symmetry constrains. The geometry of the conformer was optimized to better than 0.0001 Å for bond distances and 0.1° for bond angles. The convergence was, for all conformations and basis sets,

of at least 10^{-9} on the density matrix, and the RMS force less than 10^{-4} a. u. for the optimized structure.

IV.2.1.2 Frequencies calculations

Vibrational frequencies and IR intensities were obtained, at several basis sets, for the conformer of 2,4-DNT for comparison with the experiment. Using these data we obtained the IR vibrational spectrum of DNT. Also IR spectra were calculated for the tetrahedra surface and the DNT-tetrahedra surface interaction. We use a reduce model of the siloxane surface due the computational limitations. The resolution of the vibrational spectrum was of 4 cm^{-1}.

IV. 2.1.3 Surface site simulation

The siloxane surface was constructed out of four SiO_4 tetrahedra. It was reproduced following the specification of Bish[34,35]. In this case, the peripheral oxygen atoms of the tetrahedron SiO_4 unit were saturated with H atoms[36]. The O-Si and the O-H bond lengths are 1.6100 Å and 0.9500 Å, respectively. These bond lengths are considered the average value for clay minerals[34,35].

IV. 2.1.4 Intermolecular interaction energy

The molecular geometry of 2,4-DNT was fully optimized previous to the interaction as described previously. The siloxane surfaces of the clays were modeled within the molecular approach[37]. All ab initio calculations were accomplished with

the Gaussian 03 package of programs[7]. In this work the 6-31G, 6-31G*, 6-31+G*, 6-311G*, 6-311G (df,p) and 6-311+G* family of basis sets were used. The superimposition of the DNT on the siloxane surface was optimized employing HF and DFT methods. The optimization depended on six variables which include vertical distance, rotation and inclination angles that allowed the explosive molecule moved freely until reach the optimum adsorption site in siloxane surface.

The binding energies –or intermolecular interaction energies– were computed at the DFT, DFT//HF and MP2//HF levels of theory. The nomenclature described before, e.g. DFT//HF, implies an optimization calculation with the HF method and an energy calculation with the DFT method. The hybrid B3LYP functional[38] was used for the DFT calculations. We use the counterpoise methods to correct the binding energies for the BSSE.

IV. 2.1.5 Solvent effects on the DNT spectroscopic signature

Solvent effects for the DNT molecule were determined using water as solvent. The water dielectric constant is $\varepsilon = 78.39$. These calculations were performed at the DFT (B3LYP) method using the 6-311+G** basis set. Both the Onsager model and the Tomasi's polarized continuum solvent model PCM were carried out. In the Onsager calculations we have used the cavity radii derived from molecular volume calculations. The gas-phase molecular volume calculation was computed in a separate job step, using the called *volume* keyword in Gaussian 03 programs. The geometry

calculations of the DNT molecule was fully optimized with both solvation methods. The frequencies obtained are based on the optimized geometry, the dielectric constant of water, and an estimation of the molecular volume in the case of the Onsager reaction field model.

IV.2.2 Experimental Analysis

The FT-IR experiments were performed using a Bruker Optics IFS 66 series FT-IR spectrometer coupled with Infrared Microscopy using a photovoltaic liquid N_2 cooled MCT detector equipped with the OPUS software 4.0. The DNT standard solutions used was certified as 1000 parts per million (ppm). These solutions are dissolved in acetonitrile (ACN). The soil used for this study was obtained from the University of Puerto Rico Mayagüez campus backyard and separate in their components – clay, sand and silt– according to the USDA mechanical method[39]. X-Rays analysis was performed to the clay mineral sample and classified as Kaolinite clay mineral.

IV.2.2.1 Characterization of DNT and clay samples

DNT and clay characterization is an important step to know their main vibrational bands. We place a small amount of DNT solid in a stainless steel surface and then we proceed to analyzed it using the FT-IR microspectroscopy technique. A small amount of clay sample was placed in a stainless steel surface too and then analyzed.

IV.2.2.2 DNT and clay interaction

For the interaction we prepared a diluted solution from the DNT 1000 ppm standard solution to a concentration of 100 ppm. Then 50 μL (equivalent to 5 μg) of this 100 ppm DNT solution, were mixed with 0.0100 g of clay in microtubes of centrifuge and mixed for 60 seconds using a vortex. The DNT-clay samples have a concentration of 500 ppm. The mixed samples were then transferred to a stainless steel surfaces. After the solvent evaporated completely the samples were analyzed by the reflection FT-IR micro spectroscopic technique. No signal from the solvent was detected. The general conditions under which these analyses were carried out include a resolution of 4 cm^{-1} and 64 scans. The spectra were obtained in the 650-3800 cm^{-1} IR range.

V. RESULTS AND DISCUSSION

The principal objective of this research was to obtain the chemical signatures of the DNT explosive when it interacts with the soil, specifically with clay minerals.

A fate and transport study of TNT in soil predicts that over 90% of the explosives escaping from a landmine are adsorbed on to the soil solid phase particles, about 10% remains in the liquid phase, and only a trace (about 10^{-6}) is in the vapor phase. Therefore, a small soil particle sample collected from the surface of the ground could easily contain a much larger quantity of explosive than a large sample of air, immediately over the landmine.

To carry out our goal we performed several steps as optimize the DNT molecule to obtain a real geometry structure, to interact it with the siloxane surface of the clay minerals, and the vibrational properties. The explosives should enter in contact with water when it is in the environment. Therefore, to study the solvent effects we solvated the DNT molecule with water. This research considers the altered explosive properties as shift bands, due the interaction of it with the soil specifically with clay minerals, and the interaction energy between both.

V.1 Theoretical characterization of DNT, siloxane and the DNT-siloxane

V.1.1 Optimization of DNT molecular structure

The geometry of the 2,4-DNT was optimized in order to determine the lowest energy conformation, its structural parameters[40], and the optimized symmetry. The energy of a molecular system varies with changes in its structure and it is specified by its potential energy surface. A potential energy surface is a mathematical relationship linking molecular structure and the resultant energy. Geometry optimizations usually attempt to achieve minimum potential energy surface, thereby predicting equilibrium structures of the molecular systems[14]. To optimize the geometry we use the Gauss View visualization program. Using this program we model an initial structure of the DNT based in the typical values of the bond lengths, bond angles, and dihedral bond angles. Then the structure was fully optimized at the DFT level.

Table 5.1 presents the B3LYP optimized energies of 2,4-DNT at different basis sets, in hartrees and kcal/mol units using the Gaussian 03 program (see example of the DNT optimization z-matrix in Appendix 5.1). Among the several basis sets used for these calculations, the 6-311+G** basis set provides the lower energy conformation. The most stable geometry obtained for the DNT isomer is show in Figure 5.1. This molecule has C_1 symmetry and consists of a phenyl ring with a methyl group and two nitro groups at positions 2 and 4.

Table 5.1 Calculated DFT (B3LYP) optimized energies of 2,4-DNT.

Basis Set	3-21G	6-31G	6-31G*	6-31+G*	6-311G	6-311G*	6-311+G**
Energy (hartrees)	-676.7575	-680.3372	-680.5618	-680.5904	-680.5191	-680.7312	-680.7572
Energy (kcal/mol)	-424672.1	-426918.4	-427059.4	-427077.3	-427032.5	-427165.6	-427181.9

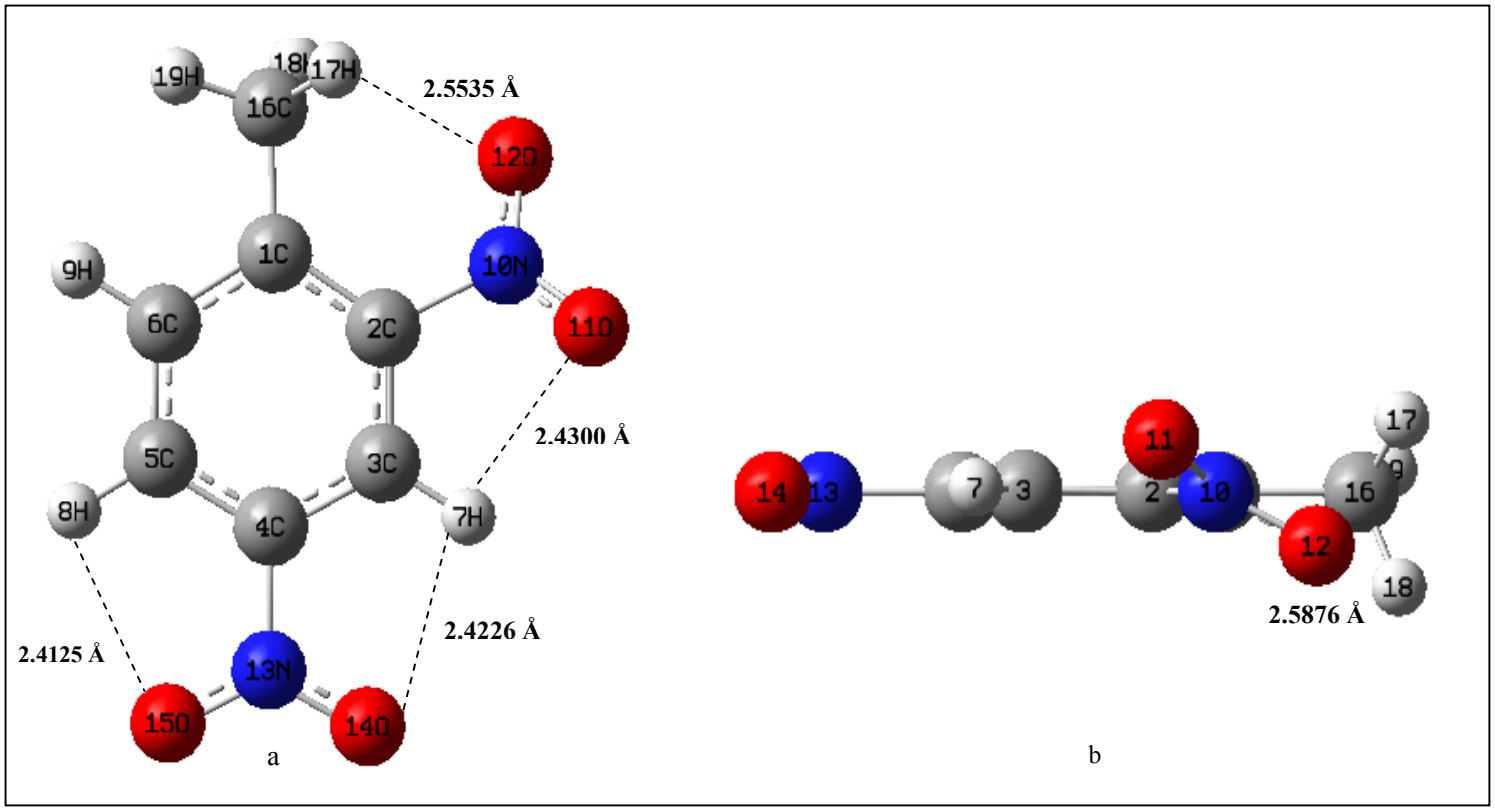

Figure 5.1 (a)Top and (b) side view of B3LYP/6-311+G** Optimized Molecular structure of 2,4-DNT

The DNT optimized structure exhibits a phenyl ring deformation due to inductive, resonance and steric effects. This phenyl ring distortion depends on the closeness of the methyl and nitro groups to each other. Also, in the absence of intramolecular interactions between them (the methyl and nitro groups) they tend to be coplanar with the phenyl ring. The nitro group in position 4, due to its far position from neighbors (no steric effects), tends to be coplanar with the ring, contrary to nitro group in position 2 that is not coplanar due the steric effects with methyl group.

An O---H separation lower than the sum of the van der Waals radii (1.4 and 1.2 Å, respectively) indicate that exist an intramolecular H-bonding. In Figure 5.1 is shown the DNT optimized structure at B3LYP/6-311+G** level of theory and basis set, respectively. The figure also shows the intramolecular interactions that are presents in the molecule. These interactions are between the O atoms of the NO_2 groups and the H atoms of the ring and CH_3 methyl group.

The DNT intramolecular interactions obtained using the B3LYP/6-31G* between the O atoms of the 2-NO_2 group and the H atoms of the CH_3 group are compare with a study performed by Chen and coworkers using HF/6-31G*. The values obtained with B3LYP are 2.4898 and 2.5310 Å between the O12-H17 and O12-H18 (see O and H atoms in Figure 5.1), respectively. The B3LYP average value was 2.5104 Å whereas the value obtained by Chen and coworkers[30] was 2.5028 Å using the HF/6-31G* methods. Experimental studies demonstrate that these intramolecular

interactions are weak. The B3LYP level is which obtained a higher value of O-H distance (closer to 2.6 Å) given an intramolecular interaction more weak than the obtained with the HF level.

The calculated structural parameters (bond lengths, angles, and dihedral angles) of the DNT are listed in Tables 5.2, 5.3 and 5.4, respectively. The labeling of the atoms in these tables is consistent with the labeling with the ball-and stick model shown in Figure 5.1. The parameters were obtained using the B3LYP method increasing the basis sets from 3-21G to 6-311+G**. Those tables also provide the parameters obtained from Chen and coworkers using the HF/6-31G* level.

The parameters obtained with the B3LYP/6-31G* basis set are compared with the values obtained by Chen and coworkers using HF/6-31G*. We can observe that the HF method used by Chen et al. (1997) underestimates the bond lengths of the DNT optimized compare structure to the DFT level of theory. The C-C, C-N, and N-O average bond lengths calculated by HF method has a lengths differences of -0.0085, -0.0170 and -0.0367 Å, respectively. However no significant differences were observed between the bond angles and dihedral angles (Table 5.3 and 5.4).

Table 5.2 Optimized B3LYP bond lengths of 2,4-DNT at different basis sets.

Bonds (Å)	Basis Sets							[30]HF/ 6-31G*
	3-21G	6-31G	6-31G*	6-31+G*	6-311G	6-311G*	6-311+G**	
C(5)-C(6)	1.3879	1.3913	1.3895	1.3910	1.3894	1.3874	1.3878	1.3793
C(4)-C(5)	1.3908	1.3967	1.3927	1.3942	1.3946	1.3897	1.3904	1.3827
C(3)-C(4)	1.3802	1.3877	1.3861	1.3879	1.3858	1.3835	1.3844	1.3758
C(2)-C(3)	1.3901	1.3969	1.3930	1.3938	1.3945	1.3898	1.3895	1.3831
C(1)-C(6)	1.4073	1.4114	1.4060	1.4069	1.4091	1.4033	1.4033	1.3948
C(1)-C(16)	1.5121	1.5083	1.5078	1.508	1.5067	1.5059	1.5056	1.5135
<CC>	**1.4114**	**1.4154**	**1.4125**	**1.4136**	**1.4134**	**1.4099**	**1.4102**	**1.4040**
H(8)-C(5)	1.0799	1.0820	1.0831	1.0837	1.0785	1.0818	1.0814	-
H(9)-C(6)	1.0827	1.0838	1.0857	1.0861	1.0804	1.0843	1.0835	-
H(7)-C(3)	1.0774	1.0807	1.0813	1.0823	1.0772	1.0801	1.0804	-
H(19)-C(16)	1.0927	1.0929	1.0936	1.0938	1.0888	1.0909	1.0907	-
H(17)-C(16)	1.0928	1.0938	1.0932	1.0940	1.0892	1.0907	1.0912	-
H(18)-C(16)	1.0928	1.0938	1.0938	1.0946	1.0897	1.0913	1.0919	-
<HC>	**1.0864**	**1.0878**	**1.0885**	**1.0891**	**1.0840**	**1.0865**	**1.0865**	**-**
C(2)-N(10)	1.4700	1.4731	1.4782	1.4783	1.4712	1.4843	1.4825	1.4611
C(4)-N(13)	1.4629	1.4661	1.4725	1.4742	1.4659	1.4797	1.4798	1.4556
<CN>	**1.4665**	**1.4696**	**1.4754**	**1.4763**	**1.4686**	**1.4820**	**1.4811**	**1.4584**
N(10)-O(11)	1.2828	1.2636	1.2289	1.2302	1.2656	1.2215	1.2225	1.1932
N(10)-O(12)	1.2832	1.2641	1.2304	1.2313	1.2668	1.2235	1.2240	1.1926
N(13)-O(15)	1.2829	1.2639	1.2300	1.2313	1.2661	1.2228	1.2237	1.1921
N(13)-O(14)	1.2815	1.2623	1.2287	1.2300	1.2646	1.2215	1.2225	1.1933
<NO>	**1.2826**	**1.2635**	**1.2295**	**1.2307**	**1.2658**	**1.2223**	**1.2232**	**1.1928**

Table 5.3 Optimized B3LYP bond angles of 2,4-DNT at different basis sets.

Angles (deg.)	Basis Sets							[30]HF/ 6-31G*
	3-21G	6-31G	6-31G*	6-31+G*	6-311G	6-311G*	6-311+G**	
C(4)-C(5)-C(6)	118.9	118.6	118.6	118.6	118.7	118.7	118.7	-
C(3)-C(4)-C(5)	121.1	121.5	121.5	121.5	121.4	121.4	121.5	-
C(2)-C(3)-C(4)	119.4	118.7	118.5	118.3	118.6	118.4	118.2	-
C(1)-C(6)-C(5)	122.0	122.6	122.7	122.7	122.6	122.6	122.5	-
C(16)-C(1)-C(6)	118.7	118.3	118.6	118.9	118.6	118.8	119.1	-
<CCC>	**120.0**	**119.9**	**120.0**	**120.0**	**120.0**	**120.0**	**120.0**	-
H(8)-C(5)-C(6)	122.4	121.7	121.7	121.5	121.7	121.6	121.6	-
H(9)-C(6)-C(5)	119.5	119.2	119.0	119.0	119.2	119.0	119.1	-
H(7)-C(3)-C(4)	120.7	121.0	121.0	121.0	121.0	121.0	121.0	-
H(19)-C(16)-C(1)	109.5	109.7	109.7	109.7	109.8	109.9	109.7	-
H(17)-C(16)-C(1)	110.9	111.7	111.9	112.1	112.0	112.2	112.0	-
H(18)-C(16)-C(1)	110.9	111.6	111.2	111.1	111.3	111.1	110.9	-
<HCC>	**115.7**	**115.8**	**115.7**	**115.7**	**115.8**	**115.8**	**115.7**	-
N(10)-C(1)-C(2)	122.8	122.2	121.8	121.4	121.9	121.7	121.3	121.7
N(13)-C(3)-C(4)	119.2	119.1	119.0	119.0	119.1	119.4	119.0	119.1
<NCC>	**122.8**	**122.2**	**120.4**	**121.4**	**121.9**	**121.7**	**121.3**	**120.4**
O(11)-N(10)-C(2)	117.1	117.8	117.4	117.5	117.9	117.3	117.7	117.3
O(12)-N(10)-C(2)	118.1	118.8	118.1	117.9	118.7	117.8	119.5	118.0
O(15)-N(13)-C(4)	116.8	117.6	117.3	117.4	117.8	117.2	117.3	117.3
O(14)-N(13)-C(4)	117.1	118.0	117.6	117.7	118.1	117.5	117.6	117.6
<ONC>	**117.3**	**118.1**	**117.6**	**117.6**	**118.1**	**117.4**	**118.0**	**117.6**

Table 5.4 Optimized B3LYP dihedral angles of 2,4-DNTat different basis sets.

Dihed. Angles (deg.)	Basis Sets							[30]HF/ 6-31G*
	3-21G	6-31G	6-31G*	6-31+G*	6-311G	6-311G*	6-311+G**	
C(3)-C(4)-C(5)-C(6)	0.0	0.0	0.0	0.2	0.0	0.1	0.2	-
C(2)-C(3)-C(4)-C(5)	0.0	0.0	0.0	-1.2	-0.4	-0.9	-1.2	-
C(1)-C(6)-C(5)-C(4)	0.0	0.0	0.0	0.9	0.5	0.8	1.0	-
C(16)-C(1)-C(6)-C(5)	-180.0	-180.0	-180.0	-179.8	-180.0	179.9	-180.0	-
H(8)-C(5)-C(6)-C(1)	-180.0	-180.0	-180.0	-179.4	-179.7	-179.5	-179.3	-
H(9)-C(6)-C(5)-C(4)	180.0	-180.0	-180.0	-179.0	-179.5	-179.3	-179.0	-
H(7)-C(3)-C(4)-C(5)	-180.0	180.0	180.0	179.0	179.2	178.8	178.8	-
H(19)-C(16)-C(1)-C(6)	0.0	0.1	0.1	10.5	7.9	9.9	12.2	-
H(17)-C(16)-C(1)-C(6)	121.0	121.0	121.0	131.4	129.1	130.9	133.2	-
H(18)-C(16)-C(1)-C(6)	-121.0	-120.8	-120.8	-109.7	-122.6	-110.5	-108.0	-
N(10)-C(2)-C(3)-C(4)	180.0	-180.0	-180.0	-179.0	-179.8	-179.2	-179.0	180.3
N(13)-C(4)-C(5)-C(6)	180.0	-180.0	-180.0	179.9	179.9	179.9	179.9	180.6
O(11)-N(10)-C(2)-C(3)	0.0	-0.2	-0.2	-24.3	-15.9	-21.7	-29.0	-
O(12)-N(10)-C(2)-C(3)	-180.0	179.9	179.9	155.0	163.7	157.6	150.3	-
O(15)-N(13)-C(4)-C(5)	0.0	0.0	0.0	-0.4	-0.4	-0.6	-0.4	-
O(14)-N(13)-C(4)-C(5)	-180.0	180.1	180.1	179.6	-180.4	179.3	179.6	-

It has long been recognized that HF theory usually gives bond lengths which are too short, and the description of multiple bonds tends to be problematic due to the neglect of electron correlation. The MP2 approach, conversely, frequently overestimate bond distances[41].

V.1.2 IR Analysis of the DNT molecular structure

In order to obtain the spectroscopic signature of the DNT molecule we performed frequency calculations for the different basis sets. The theoretical frequencies obtained for the DNT with the higher basis set (6-311+G**) are in good agreement with their experimental frequencies. This work present the vibrational frequencies of the most stable geometry observed. These frequencies have to be real, or positive to consider that the geometry reach a minimum.

DNT simulated spectrum obtained using the B3LYP/6-311+G** calculation is compared against the experimental spectrum in Figures 5.2, 5.3 and 5.4 at ranges of 600-1200, 1300-1700 and 2800-3300 cm^{-1} respectively. There are several discrepancies between the theoretical and experimental spectra in Figure 5.2. Some of the experimental resolved vibrational bands appear overlapped in the calculated spectra. For example the ring out of plane (oop) bend at 648 cm^{-1}, the ring in plane (ip) stretch and CH_3 stretch at 804 cm^{-1}; the C-H (ring) and CH_3 oop bend at 850 cm^{-1}; and the 2,4-NO_2 scissoring and ring ip stretch at 854 cm^{-1}. In the experimental

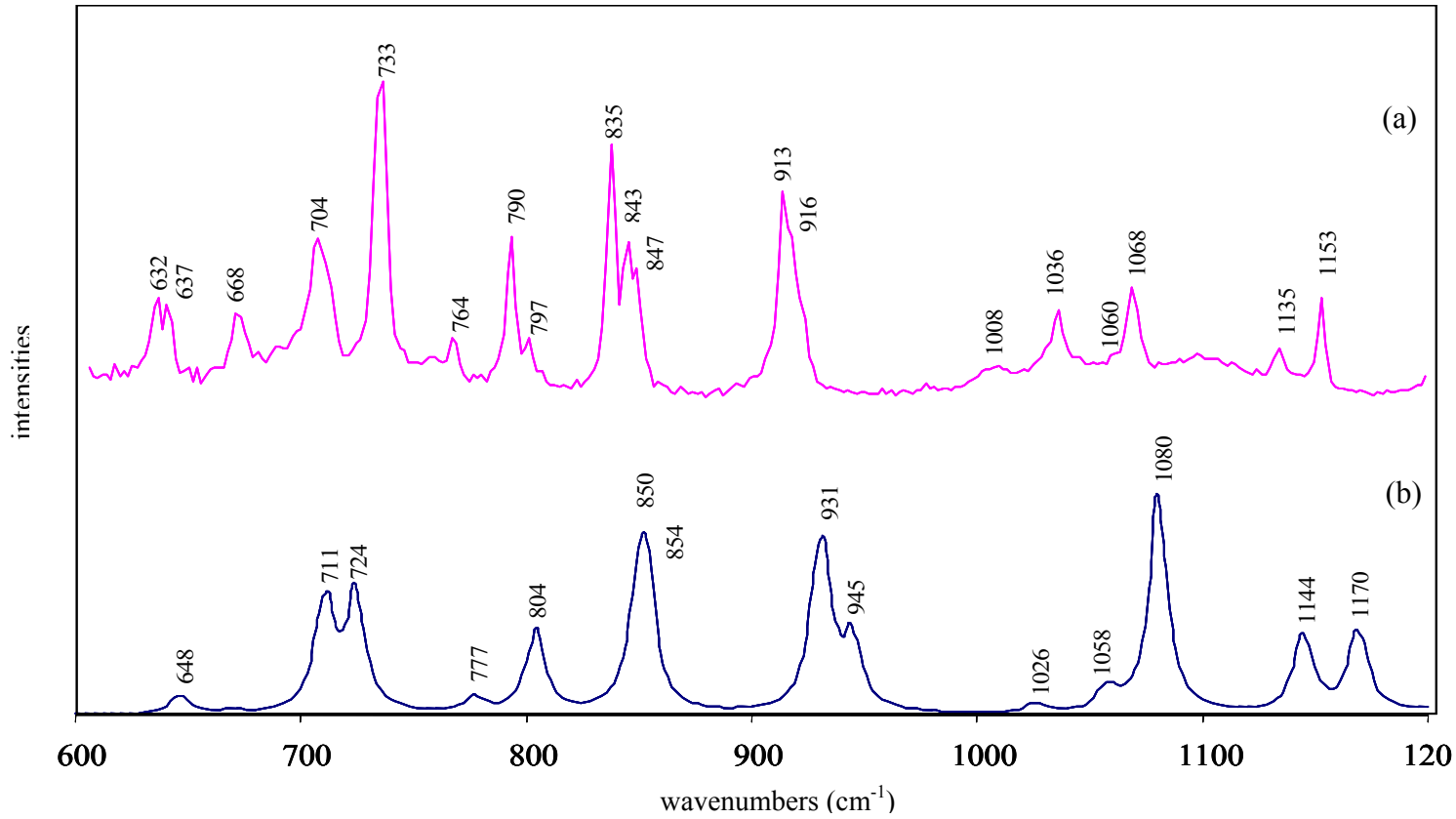

Figure 5.2 (a) Experimental and (b) theoretical (B3LYP/6-311+G**) IR spectra of DNT from 600 to 1200 cm^{-1}

spectrum the 648 cm^{-1} band appears at 632 and 637 cm^{-1}, the 804 cm^{-1} band appears at 790 cm^{-1} and 797 cm^{-1}, whereas the 850 and 854 cm^{-1} correspond to the 835, 843 and 847 cm^{-1} bands. A reverse case is presented on experimental spectrum where at 913 and 916 cm^{-1} vibrational bands are not resolved as the theoretical corresponding bands at 931 cm^{-1} for 2,4-NO_2 scissoring and ring ip bend and at 945 cm^{-1} for C-H oop wagging.

In addition we can observe, in the theoretical spectrum, red shifts at the bands describe above. Other vibrational bands that present red shifts are localized at 711 cm^{-1} (4 C-N oop bend and ring bend), 777 cm^{-1} (CH_3 wagging, 2,2 C-N twist and ring oop bend) , 1026 cm^{-1} (CH_3 rocking and ring ip bend) , 1080 cm^{-1} (ring C-H ip bend and ring ip bend) , 1144 cm^{-1} (2,4 C-N stretch, methyl rock and ring ip stretch), and 1170 cm^{-1} (ring C-H ip bend). These vibrational bands in the experimental spectrum correspond to the 704, 764, 1006, 1068, 1135 and 1153 cm^{-1} bands, respectively. A blue shift vibrational band can be seen in the theoretical spectrum at 724 cm^{-1} which appear at 733 cm^{-1} in the experimental spectrum. This vibrational mode corresponds to the 4-CN oop bend and C-H (ring) wagging.

As can be seen in Figure 5.3, the features of the DNT vibrational spectra are reproduce very well at the region of 1300-1700 cm^{-1}. The NO_2 symmetric and asymmetric stretching region is modeled remarkably well.

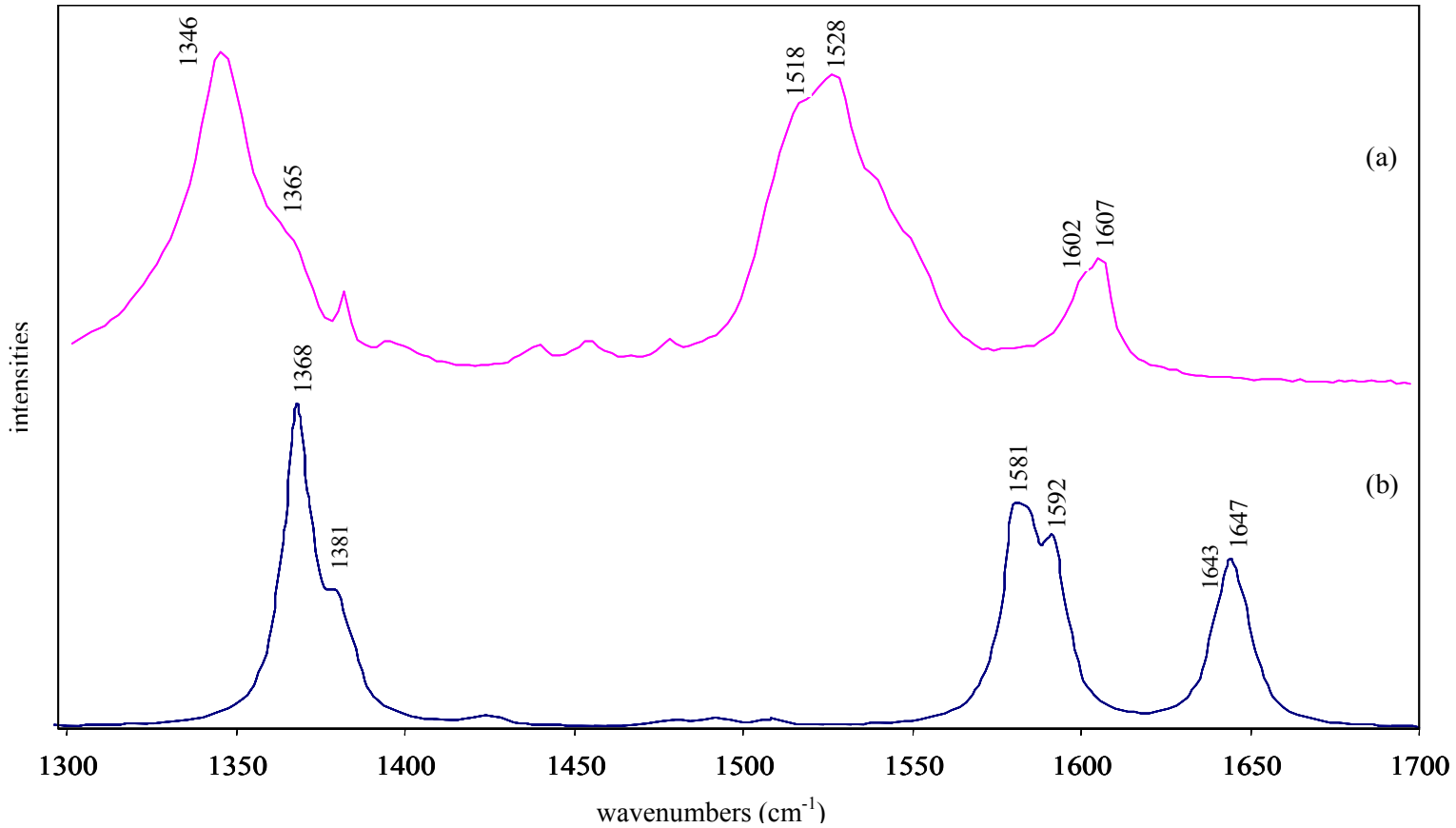

Figure 5.3 (a) Experimental and (b) theoretical (B3LYP/6-311+G**) IR spectra of DNT from 1300 to 1700 cm^{-1}

In the theoretical spectrum of DNT the NO_2 symmetric peaks appears at 1368 and 1381 cm^{-1}, and the NO_2 asymmetric peaks are observed at 1581 and 1592 cm^{-1}. In the experimental spectrum these peaks are observed at 1346 cm^{-1} and 1365 cm^{-1}, and at 1518 and 1528 cm^{-1}, respectively. The peaks at 1643 cm^{-1} and 1647 cm^{-1} in the theoretical spectrum are observed at 1602 cm^{-1} and 1607 cm^{-1} in the experimental spectrum. These vibrational bands are attributing to the ring and asymmetric 2-NO_2 stretching coupled. The entire theoretical spectrum in this range shows red shifts in comparison with the experimental spectrum.

Figure 5.4 presents the range of 2800-3300 cm^{-1}. In the experimental spectrum the band at 2871 cm^{-1} correspond to the methyl C-H, meanwhile the bands at 3057, 3088, and 3105 cm^{-1} correspond to the ring C-H stretching. In the theoretical spectrum the vibrational modes at 3050, 3109, and 3124 cm^{-1} peaks correspond to the methyl C-H stretching. Whereas the vibrational bands at 3186, 3223, and 3238 cm^{-1} correspond to the ring C-H stretching. These bonds have sp^2 hybridization, whereas, the methyl C-H bonds have sp^3 hybridization. As higher is the hybridization degree and the bond length, lower is the bond force and therefore, the frequencies. Consequently, the methyl C-H vibrations appear at lower frequencies than the ring C-H vibrations.

Table 5.5 displays the main vibrational frequencies (see all vibrational modes in Appendix 5.2) of DNT obtained through theoretical calculations (at B3LYP level

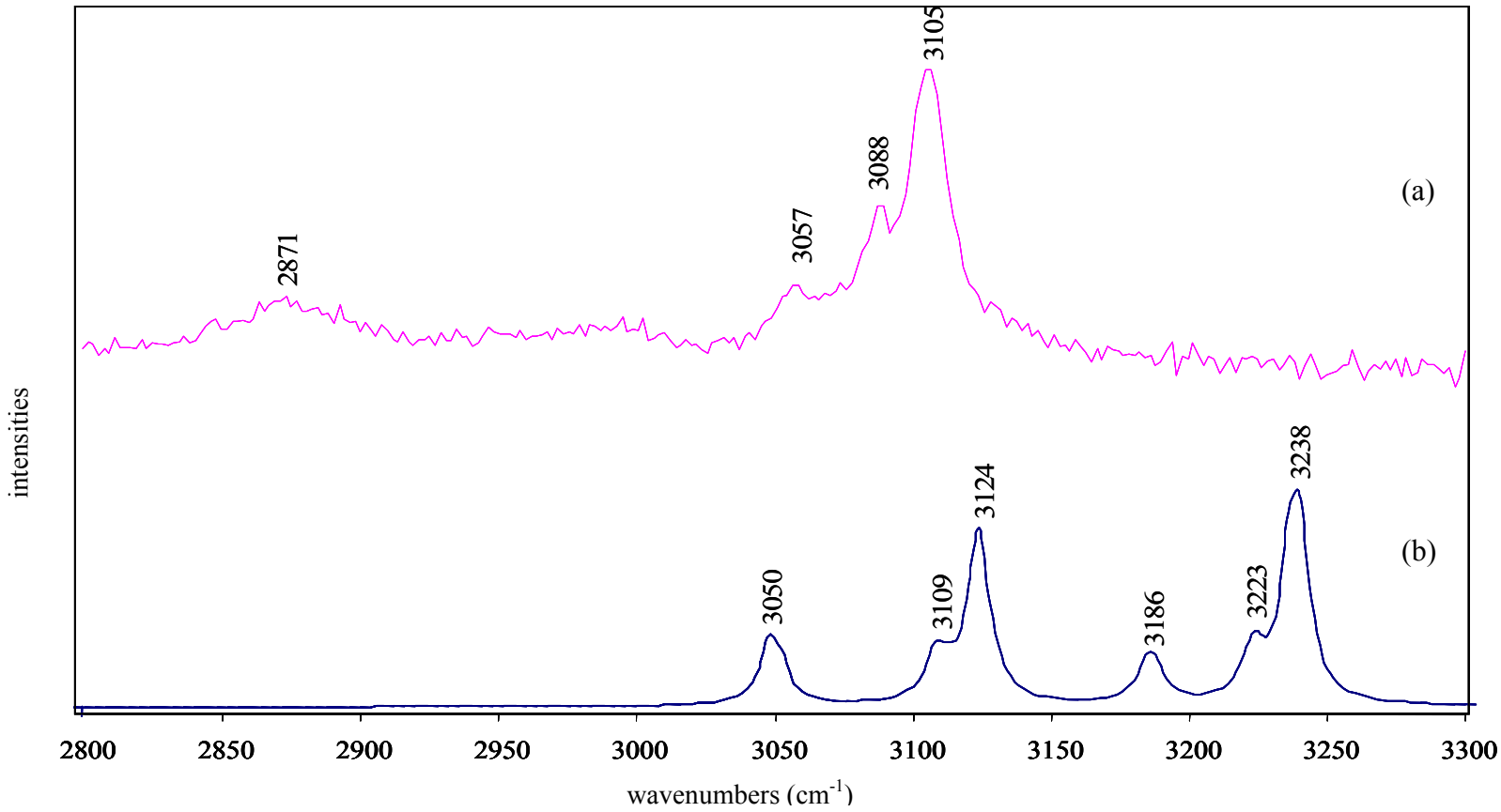

Figure 5.4 (a) Experimental and (b) theoretical (B3LYP/6-311+G**) IR spectra of DNT from 2800 to 3300 cm^{-1}

Table 5.5 B3LYP and FT-IR values of vibrational frequencies for the scissoring, symmetric and asymmetric nitro groups of 2,4-DNT.

Bands	υ	Basis Sets							Exp.
		3-21G	6-31G	6-31G*	6-31+G*	6-311G	6-311G*	6-311+G**	
Sciss. NO_2	21	761	792	801	800	787	857	854	843
	22	769	810	847	842	801	933	931	913
Sym. NO_2 stretch	35	1128	1273	1392	1381	1273	1375	1368	1346
	36	1170	1288	1404	1392	1285	1386	1381	1365
Asym. NO_2 stretch	42	1345	1428	1613	1595	1418	1597	1581	1518
	43	1348	1466	1632	1607	1463	1611	1592	1528

with several basis sets) and using the FT-IR microspectroscopy technique. The assigned bands correspond to scissoring, symmetric, and asymmetric NO_2 modes for the explosive molecule. The higher basis set, 6-311+G**, gives closer vibrational frequencies values for the NO_2 groups in comparison with the experimental values.

We can observed that the DNT theoretical spectrum present a red shift in comparison with the experimental spectrum. This shift is because the theoretical frequencies are harmonics and the experimental frequencies are anharmonics. The harmonic frequencies did not count with the anharmonic corrections which lower the frequencies.

Table 5.6 provides all the calculated vibrational frequencies at the B3LYP/6-311+G** level and basis set, respectively, corresponding infrared intensities, experimental vibrational frequencies and band assignments.

Table 5.6 B3LYP/6-311+G** theoretical and experimental vibrational frequencies and the tentative assignments for DNT molecule.(oop= out of plane, ip= in plane)

ν	B3LYP/6-311+G**		IR Freq.	IR Freq.	Assignments
	Freq	Int.	(Exp.)	(Lit.)	
1	43	0			4 NO_2 twist
2	49	0			2 NO_2 twist
3	105	0			CH_3 wagging
4	150	2			Ring oop bend
5	164	4			2,4 NO_2 rocking
6	186	1			CH_3 rotation
7	272	1			2,4 NO_2 and CH_3 rocking
8	287	2			CH_3 and ring wagging
9	343	1			CH_3 rocking, 2 C-N stretching, Ring ip stretch
10	351	1			Ring ip stretch
11	394	0			Ring oop bend
12	436	1			CH_3 rocking, Ring oop bend
13	486	6		482	CH_3 and C-H (ring) wagging
14	532	3		525	4 C-N rocking, Ring oop bend
15	575	0		632	CH_3 ip bend, 2,4 CN rocking
16	646	4		637	Ring oop deformation
17	668	0	668	668	CH_3 and C-H (ring) wagging
18	711	22	704	709	4 C-N oop bend, Ring bend
19	724	23	733	734	4 C-N oop bend, C-H (ring) wagging, ring oop bend
20	777	3	764	765	CH_3 wagging, 2,4 C-N twisting, Ring oop bend
21	804	16	790	791	Ring ip stretch, CH_3 stretch
22	850	18	835	836	C-H (ring) and CH_3 oop bend
23	854	22	843	843	2,4 NO_2 scissors, Ring ip stretch
24	931	35	913	913	2,4 NO_2 scissors, Ring ip stretch
25	945	14	916		C-H (ring) oop wagging
26	998	0			C-H (ring) oop twist, CH_3 wagging
27	1026	1	1008		CH_3 rock, ring ip bend
28	1058	4	1060	1036	CH_3 and C-H (ring) waging
29	1080	43	1068	1069	C-H ip bend, ring ip bend
30	1144	15	1135	1135	2,4 C-N stretch, ring ip stretch, methyl rock
31	1170	17	1153	1154	C-H ip bend
32	1219	6	1204	1204	Ring breathing, C-H (ring) ip bend
33	1288	7	1268	1270	C-H (ring) ip bend
34	1347	0			Ring asymmetric stretching
35	1368	431	1346	1349	2,4 NO_2 symmetric stretching
36	1381	126	1365	1383	2,4 NO_2 symmetric stretching
37	1420	1	1395	1395	CH_3 umbrella deformation
38	1425	12	1440	1440	CH_3 umbrella deformation
39	1479	8	1455	1455	CH_3 deformation
40	1492	10	1479	1479	CH_3 deformation
41	1507	8			C-H (ring) ip bend
42	1582	227	1518		2,4 NO_2 asymmetric stretching, Ring ip bend
43	1592	161	1528	1531	2,4 NO_2 asymmetric stretching, Ring ip stretch
44	1643	128	1602	1608	2,4 NO_2 asymmetric stretching, Ring ip bend
45	1647	81	1607	2870	2 NO_2 asymmetric stretching, Ring ip stretch
46	3050	6	3057	3057	C-H (methyl) symmetric stretching
47	3109	4	3088	3087	C-H (methyl) asymmetric stretching
48	3124	15	3105	3106	C-H (methyl) asymmetric stretching
49	3186	5	3128		C-H (ring) stretching
50	3223	4			C-H (ring) stretching
51	3238	19			C-H (ring) stretching

V.1.3 IR spectra of the DNT and siloxane interaction

Through the calculations we can obtained the vibrational frequencies and IR intensities of the DNT, siloxane tetrahedra surface and DNT-siloxane tetrahedra surface complex (Figure 5.5). The reason to use a reduce model of the siloxane surface (tetrahedra) is for computational limitations.

Figures 5.6, 5.7 and 5.8 show the 2,4-DNT, 2,4-DNT-tetrahedra surface and tetrahedra IR spectra separated in 650-1200 cm $^{-1}$, 1300-1750 cm $^{-1}$, and 3000-3350 cm $^{-1}$ spectral range. These spectra were obtained using DFT (B3LYP) level of theory at 6-31+G* basis set. We can observe that band shifting mainly in the 1300-1750 cm^{-1} region, where the NO_2 vibrational bands are depicted.

Figure 5.6 shows the range from 650 to 1200 cm^{-1}. The DNT-tetrahedra interaction spectrum presents blue shifts on the DNT feature peaks of -8 cm^{-1}, -3 cm^{-1}, -8 cm^{-1} and -11 cm^{-1}. The resulting vibrational bands are localized at 732 cm^{-1} (4-CN oop bend and ring C-H wagging), 839 cm^{-1} (2,4-NO_2 scissoring and ring ip stretch), 846 cm^{-1} (ring C-H oop twist, CH_3 wagging) and 942 cm^{-1} (ring C-H oop wagging). Also display other DNT feature peaks with red shifts of 4 cm^{-1} at 804 cm^{-1} which correspond to the ring ip stretch and CH_3 stretch; and of 1 cm^{-1} at 1089 cm^{-1} which is assigned to the C-H ip bend and ring ip bend.

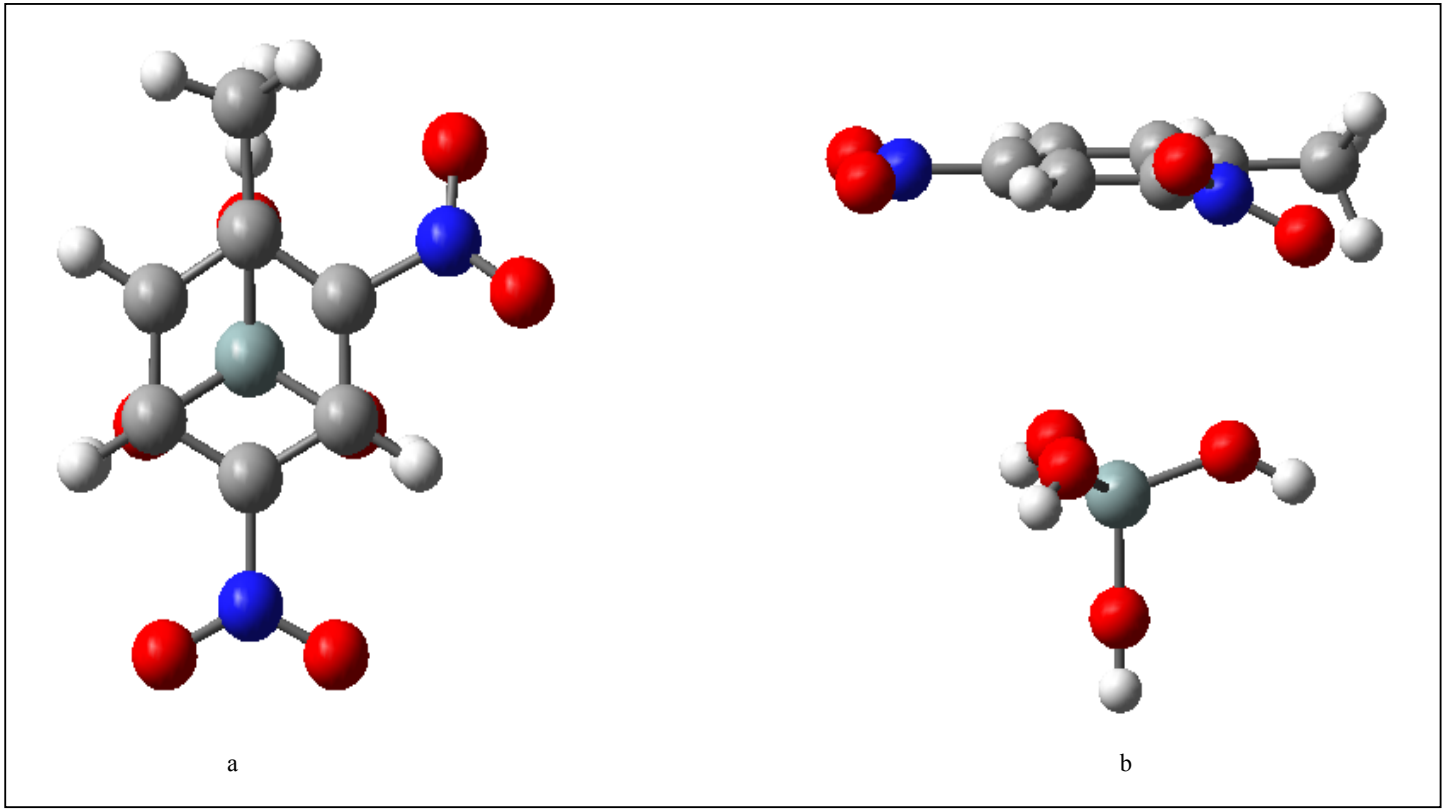

Figure 5.5 (a) Top and (b) side view of the DNT and SiO_4 tetrahedra interaction.

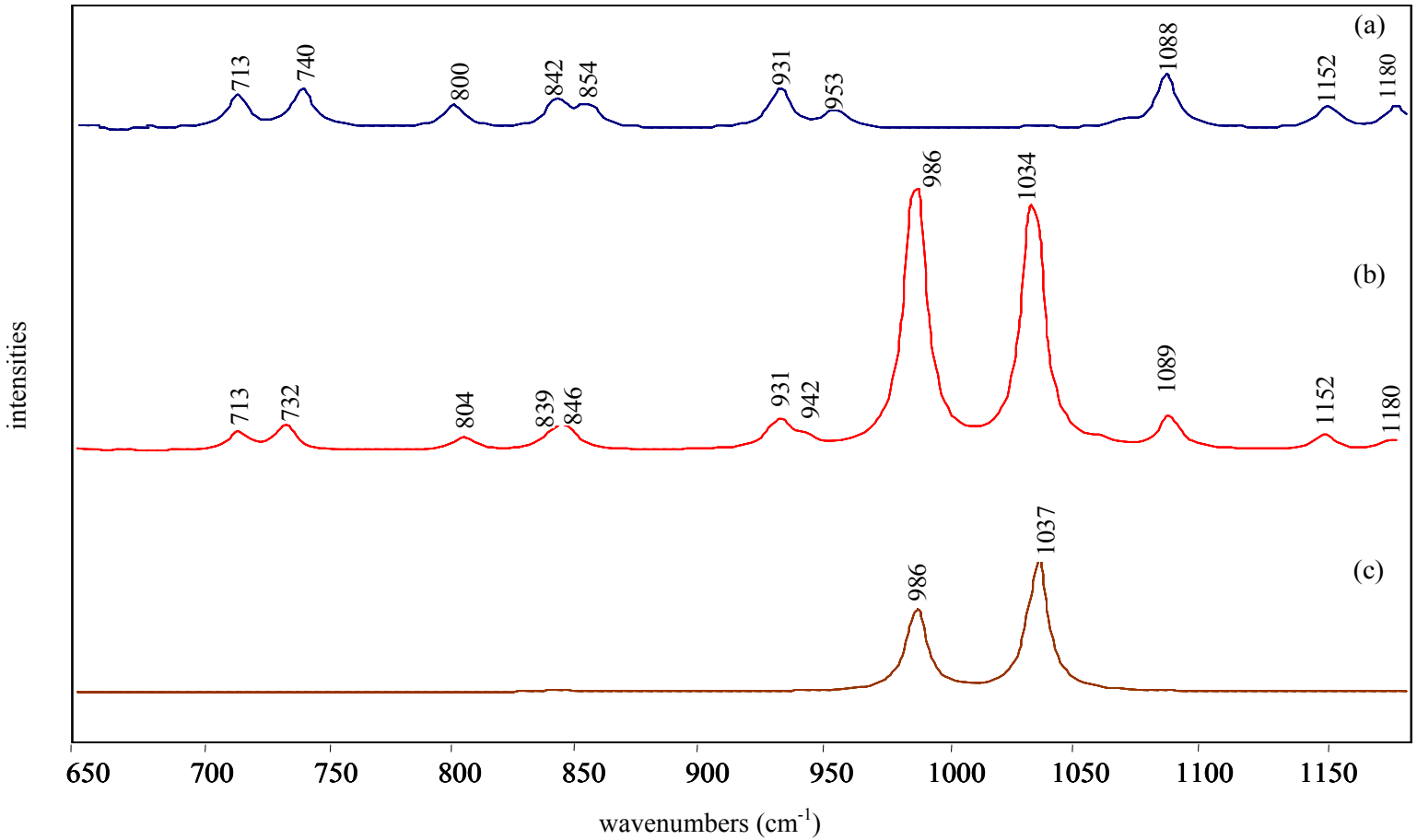

Figure 5.6 B3LYP/6-31+G* IR spectra of (a) DNT, (b) DNT-tetrahedra and (c) tetrahedra from 650 to 1200 cm^{-1}

The feature peaks of the surface model at 986 cm^{-1} and 1037 cm^{-1} are assigned to the stretch Si-O. These vibrational bands increase their intensities in the DNT-surface interaction and the band of 1037 cm^{-1} appear at low frequency (1034 cm^{-1}). The surface model does not present all feature peaks, as you will appreciate in the experimental spectrum.

The spectra in the region of 1300 to 1750 cm^{-1} shows band shifting in Figure 5.7. The band shifting corresponds to the vibrational frequencies of the NO_2 symmetric and asymmetric stretching modes. The 2,4-DNT has a symmetric NO_2 bands at 1381 cm^{-1} and 1392 cm^{-1} and asymmetric NO_2 bands at 1594 cm^{-1} and 1607 cm^{-1}. In the 2,4-DNT-tetrahedra interaction spectra these bands are observed at 1409 cm^{-1} and 1421 cm^{-1} for symmetric stretch while the asymmetric modes are observed at 1626 cm^{-1} and 1647 cm^{-1}. The 1654 and 1658 cm^{-1} vibrational bands correspond to the NO_2 asymmetric stretching coupled to ring vibrations. These bands present red shifts of 26 cm^{-1} and 30 cm^{-1}, respectively (Table 5.7).

As we note the symmetric and asymmetric NO_2 IR spectral region is excellent to identify the behavior of the interaction between DNT and soil clay minerals because clay minerals does not absorb in this region and DNT band shifting can be easily monitored.

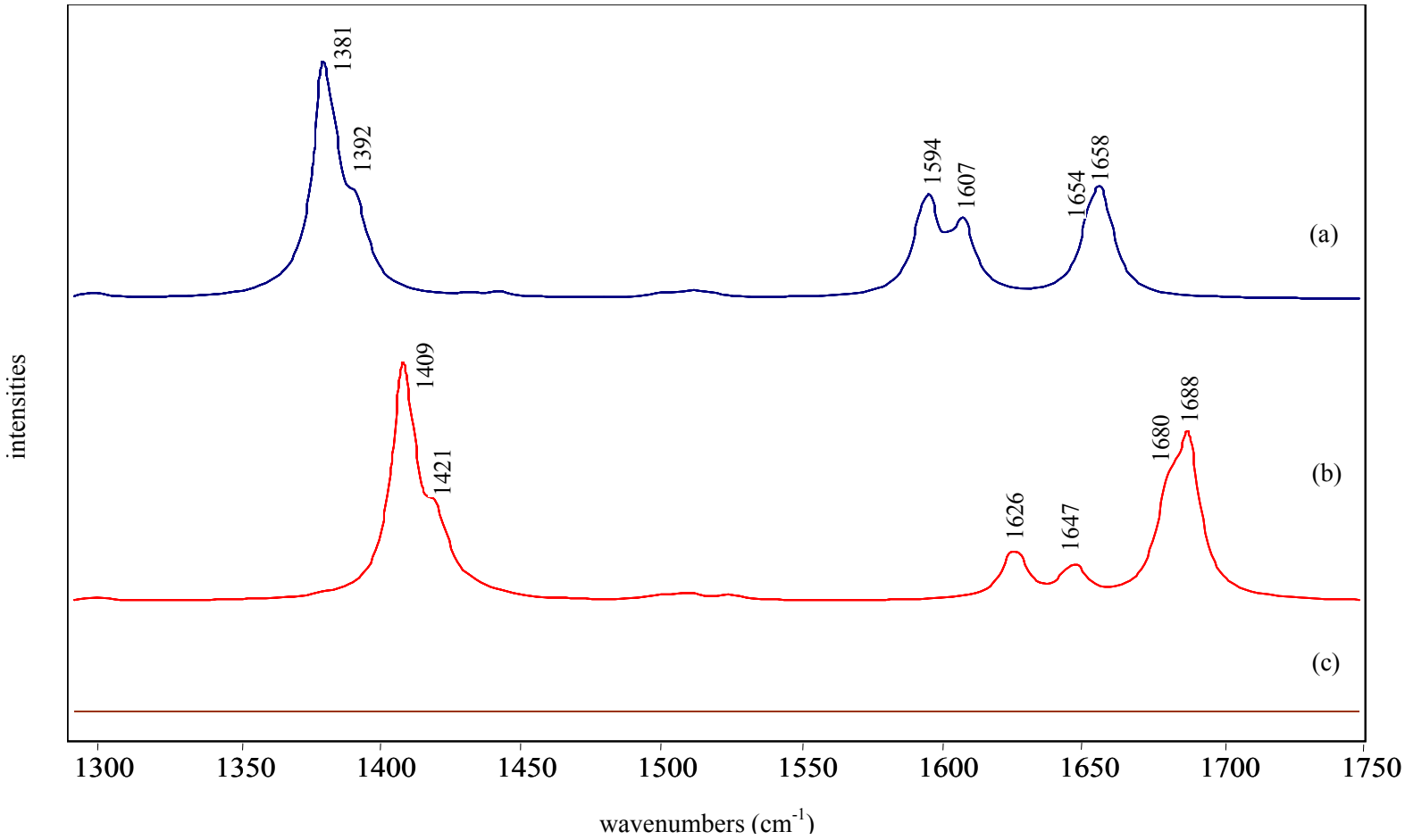

Figure 5.7 B3LYP/6-31+G* IR spectra of (a) DNT, (b) DNT- tetrahedra and (c) tetrahedra from 1300 to 1750 cm^{-1}

Table 5.7 B3LYP/6-31+G* Theoretical NO_2 vibrational frequencies of DNT and DNT/tetrahedra interaction.

Bands	**DNT**	**DNT/tetrahedra**	Δ
Asymm. NO_2	1381	1409	28
	1392	1421	29
Symm. NO_2	1594	1626	32
	1607	1647	40
Ring-NO_2 coupled	1654	1680	26
	1658	1688	30

The 3000-3350 cm^{-1} region, showed in Figure 5.8, present the C-H vibrational modes of the methyl group and the aromatic ring. The methyl C-H vibrational bands were red shifted at 3091 cm^{-1} (24 cm^{-1}), 3155 cm^{-1} (24 cm^{-1}), and 3166 cm^{-1} (25 cm^{-1}) in the DNT-tetrahedra interaction spectrum. Equally the ring C-H vibrational bands were shifted to a lower frequencies of 3228 cm^{-1} (22 cm^{-1}), 3268 cm^{-1} (20 cm^{-1}) and 3284 cm^{-1}(16 cm^{-1}).

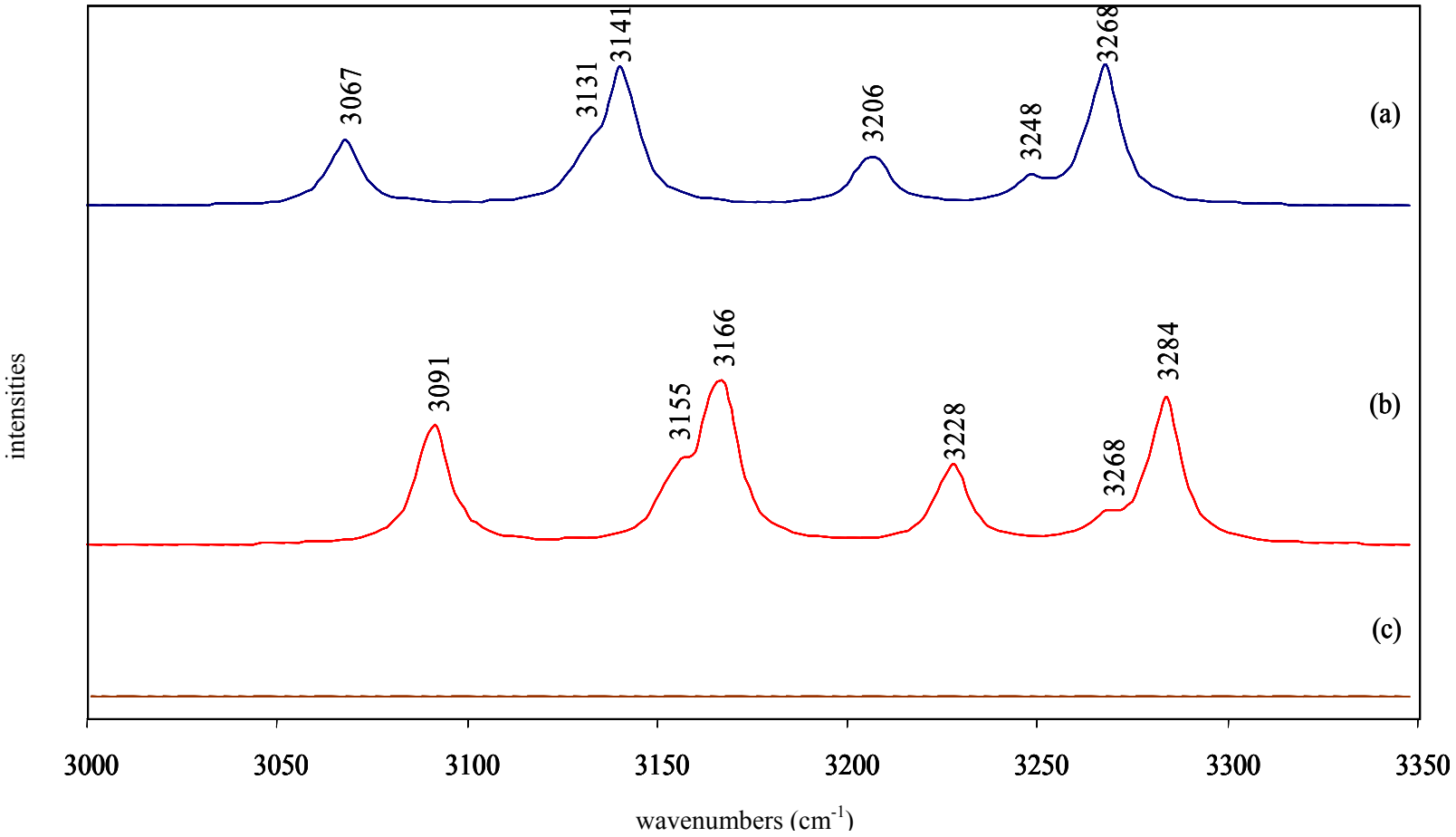

Figure 5.8 B3LYP/6-31+G* IR spectra of (a) DNT, (b) DNT-tetrahedra and (c) tetrahedra from 3000 to 3350 cm^{-1}

V.2 Experimental characterization of DNT, clay and the complex DNT-clay

V.2.1 FTIR Microspectroscopic signature of DNT in clay soils

Infrared spectroscopy provides information at the molecular level on the structure and properties of compounds. FTIR microscopy was used to investigate the chemical signature of DNT in clay soils and to observe possible interactions. This clay was obtained from soil collected at UPR, Mayagüez Campus. The clay consisted mostly of Kaolinite[39]. Clays are the most reactive component of soils. IR spectra were collected to determine the vibrational spectra of the explosive material, clay, and DNT-clay complex. These spectra are presented in three different ranges: 650-1200 cm^{-1}, 1300-1750 cm^{-1} and 2800-3800 cm^{-1} in order to facilitate the analysis of the vibrational modes of DNT, DNT-clay, and the clay. Also each vibrational spectra presents its own scale of intensity.

Figure 5.9 shows the FTIR spectra of the fundamental modes of DNT, DNT-clay complex and clay in the spectral range of 650 to 1200 cm^{-1}. This range does not present in DNT-clay spectrum any vibrational feature of DNT pure but show the clay features. Is remarkable the broader of the clay bands that should be a reason for the DNT features can not appear at this range. Other reason can be the lower concentration of the sample (500 ppm).

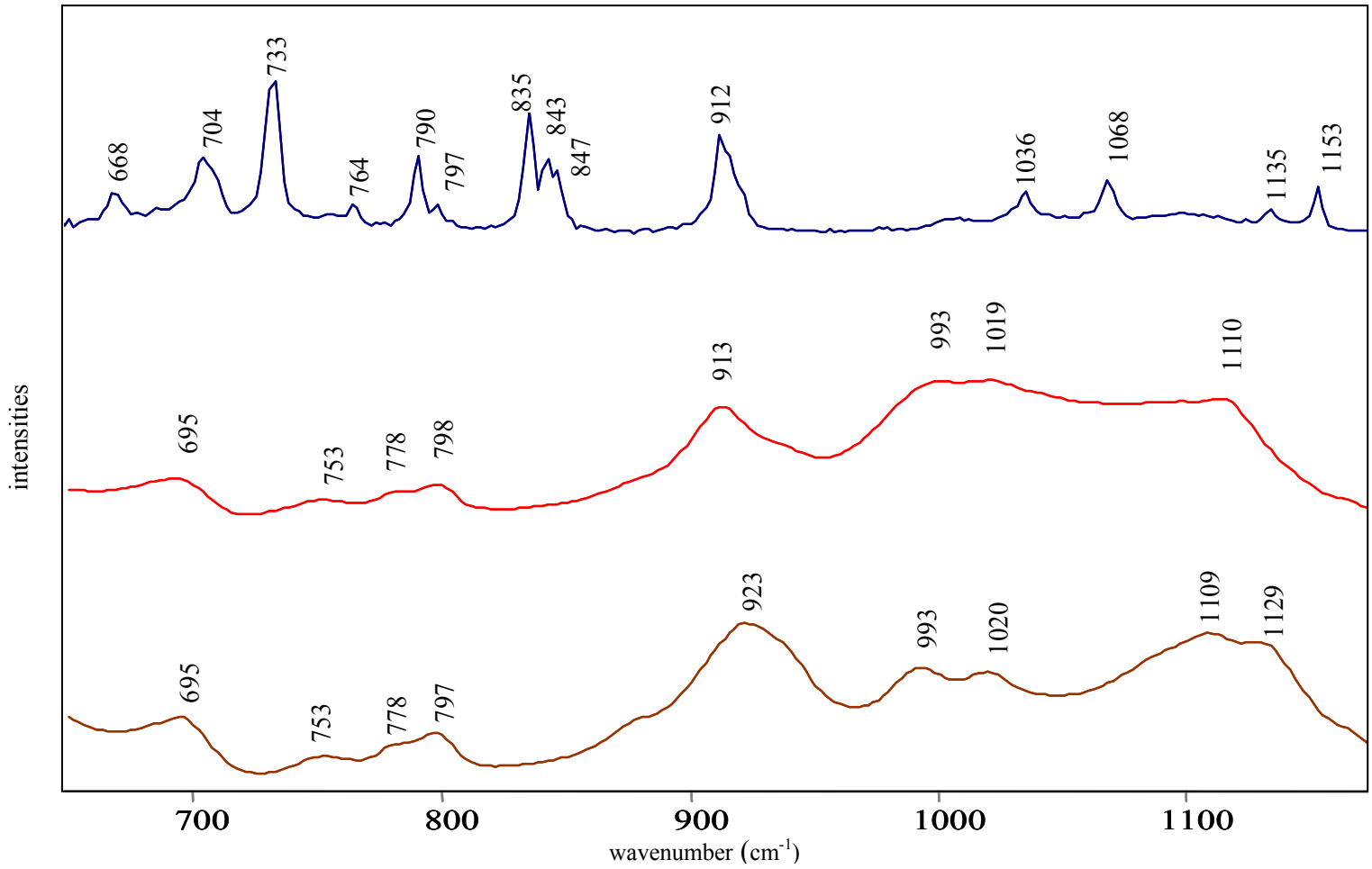

Figure 5.9 Experimental IR spectra of (a) DNT, (b) DNT-clay (500 ppm) and (c) clay from 650 to 1200 cm^{-1}

The bands assignment for DNT in this range correspond to C-N twisting, 2,4-NO_2 scissors and CH_3 deformation. Meanwhile, the characteristics clay bands are assigned as Si-O stretching[31].

Figure 5.10 covers the spectral range from 1300 to 1750 cm^{-1}. This region represents the NO_2 symmetric and asymmetric stretching fundamental modes of DNT. The DNT spectrum shows the NO_2 bands at 1346 and 1365 cm^{-1} for the symmetric mode; 1518 and 1528 cm^{-1} for asymmetric mode. Differences associated with the symmetric and asymmetric NO_2 bands are seen in the DNT-clay spectrum, with respect to the DNT spectrum. This range presents a red shift of 5 cm^{-1} at 1351 cm^{-1} for symmetric modes and for the asymmetric modes show red shift of 9 cm^{-1} at 1537 cm^{-1}. The symmetric and asymmetric NO_2 peaks of the interaction were compared with the corresponding higher peak in the DNT spectrum.

We attribute those shifts to the interaction between the explosive molecule and the clay mineral. The NO_2 modes intensities decrease a little in the interaction spectrum. Equally as we note in theoretical spectra, the clay spectrum does not absorb IR radiation in the nitro group range. Therefore, it is a good region to identify the spectroscopic signature of DNT on soil environments. The 1602 and 1607 cm^{-1} vibrational frequencies that correspond to the DNT ring and NO_2 coupled stretching are shifted at 1606 and 1615 cm^{-1}. The 1638 cm^{-1} vibrational band that corresponds to the clay is not shifted.

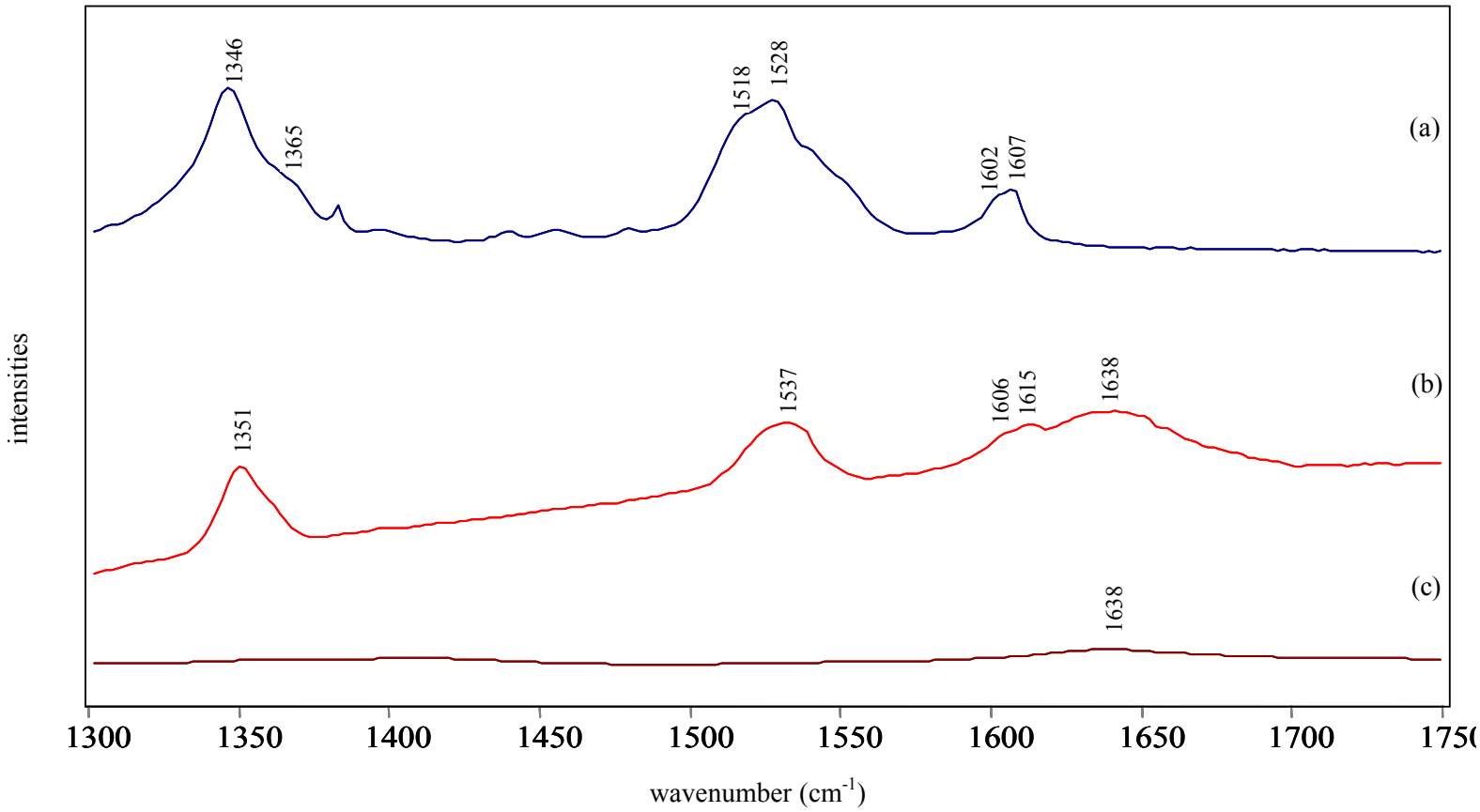

Figure 5.10 Experimental IR spectra of (a) DNT, (b) DNT-clay (500 ppm) and (c) clay from 1300 to 1750 cm^{-1}

The FTIR spectra in the range from 2800 to 3800 cm^{-1} presented in Figure 5.11 correspond to the C-H stretching bands of DNT and the O-H bands of the clay. In this region, the DNT-clay complex does not show any signals or indication of physical or chemical interaction between the DNT and clay. In this range we do not observe any DNT bands corresponding to the C-H. This is due the lower concentration of the sample of 500 ppm that corresponds to 5 μg of DNT in 0.0100 g of clay.

As we observe, with a lower concentration of 500 ppm of the DNT-clay sample, we can obtain only the symmetric and asymmetric NO_2 vibrational modes of the DNT, because are the most intense peaks. We can considerer the 1300-1700 cm^{-1} range as the spectroscopic region appropriate to detect the explosive in the soil.

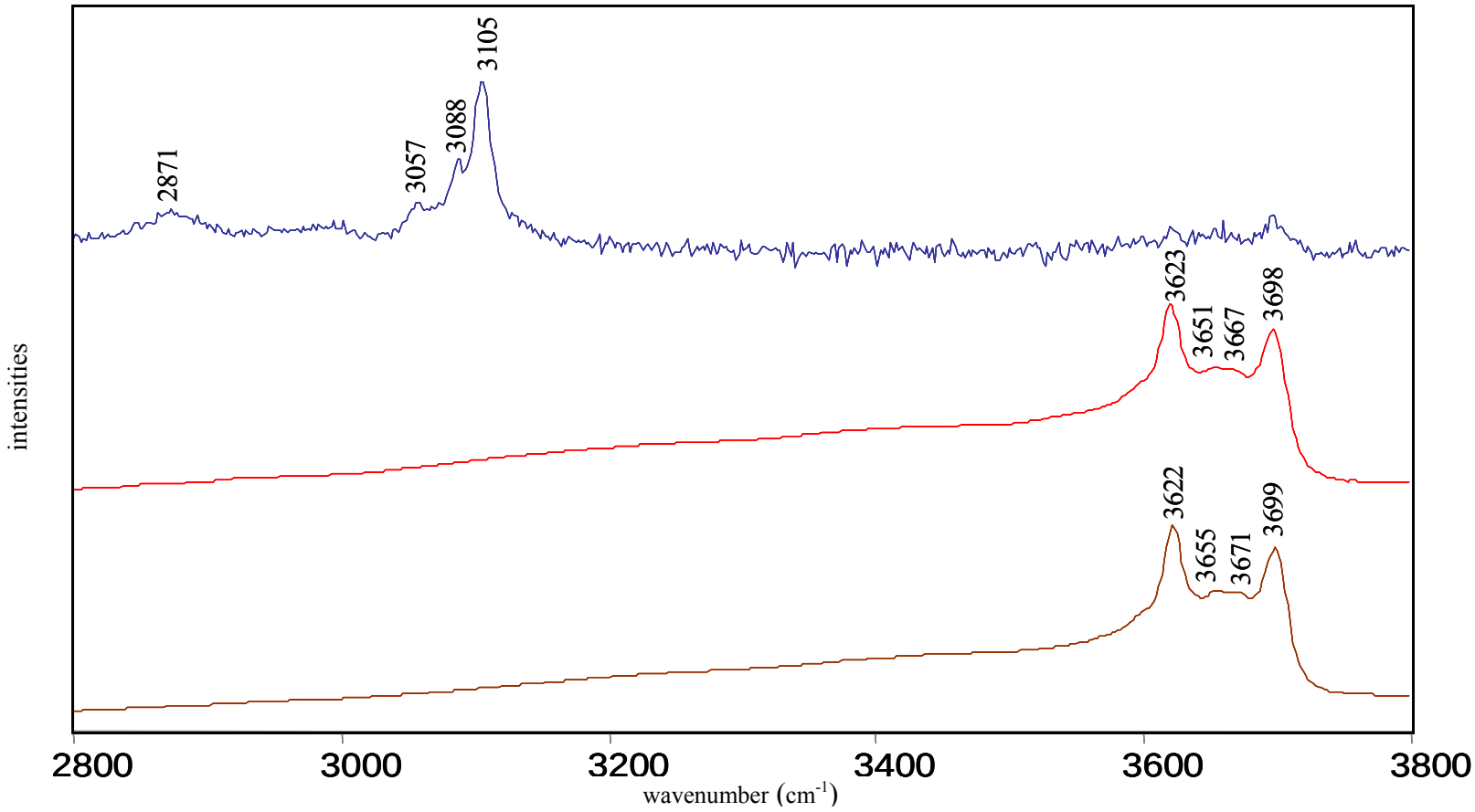

Figure 5.11 Experimental IR spectra of (a) DNT, (b) DNT-clay (500 ppm) and (c) clay from 2800 to 3800 cm^{-1}

V.3 Intermolecular interaction energy of the DNT-siloxane surface complex

One of the major difficulties involved in a quantum mechanical study to describe the interactions between molecules and surfaces lays on the fact that the surface infinite size cannot be directly computed using quantum mechanical techniques. However, this may be overcome reducing the system using a unit cell. A quantum chemical level of approximation that is adequate to provide a trustable description of intermolecular interactions needs to be to taken into account. In addition, the quantum chemical data obtained need proper corrections in order to relate them to observed quantities[37].

The siloxane surface of clays was modeled, as show in Figure 5.12, with four SiO_4 tetrahedra links through the basal oxygen's and those were saturated with H atoms in order to simulate the broken Si-O interaction between the border O atoms with the Si atoms of the following tetrahedra.

The interaction was performed with the superimposition of the DNT optimized molecule on the siloxane surface as shown in Figure 5.13a. First we optimized this interaction with the HF method at different basis sets. The optimization depended on six variables (including bond lengths, bond angles, and dihedral angles) that allowed the explosive molecule moved freely until reach the optimum adsorption site.

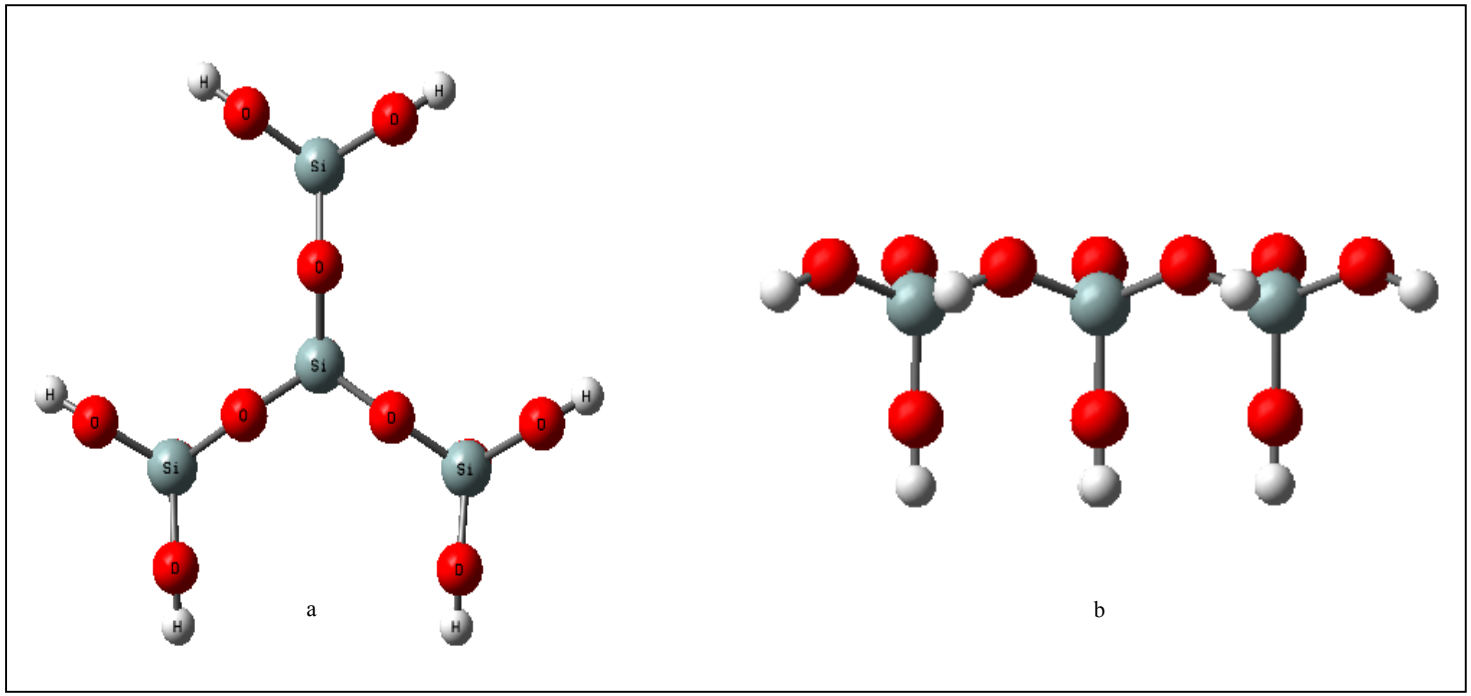

Figure 5.12 (a) Top and (b) side view of siloxane surface.

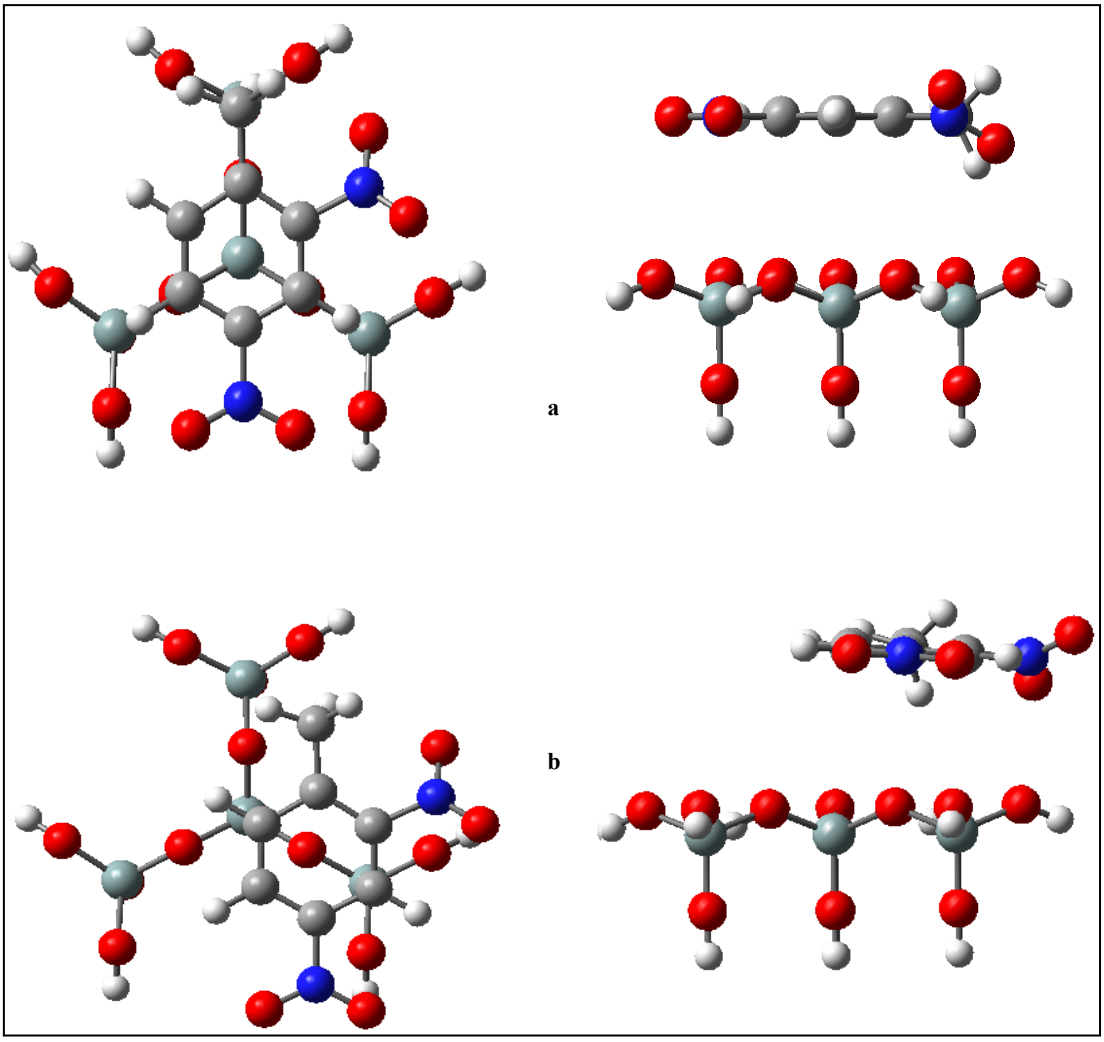

Figure 5.13 (a) Superimposition of 2,4-DNT on siloxane surface for the interaction and (b) 2,4-DNT optimized adsorption at the siloxane surface using HF/6-311+G** method. Left: Top view and right: side view.

This interaction shows the DNT molecule shifting to one side of the siloxane surface (Figure 5.13b). In Table 5.8 we show the optimized variables of the structural parameters that correspond to the interaction movements between the DNT and the siloxane surface. These movements belong to vertical distance (B1), inclination angles (A1, A2), and rotation angles (D1, D2, D3). These structural parameters give rise to the adsorption site of the DNT on the siloxane surface show in Figure 5.13b. These calculations were performed using the HF method at several basis sets.

In order to determine which phenomena govern or contribute the most to the spectroscopic signature of DNT in soil environments we use the model show in the Figure 5.13 to simulate that interaction by means of computational algorithms. In Table 5.9 we report the HF, DFT//HF and BSSE corrected DFT//HF binding energies calculated for the optimized complexes at different basis sets and the vertical distance (VD) at which we obtained the minimum energy.

The DFT//HF imply a single point calculation using the DFT approximation next to the optimization performed with the HF method. The difference between the HF and DFT//HF binding energies is small. We can conclude that the inclusion of electron correlation within the DFT approximation does not significantly affect the binding energy (E_b). The E_b values using DFT//HF method corrected with the BSSE are lower by a factor of 2 in comparison with the values obtained using the DFT//HF uncorrected. It demonstrates that it is necessary the BSSE correction.

Table 5.8 HF Optimized structural parameters that involved vertical distance, rotation and inclination angles between the 2,4-DNT and the siloxane site surface

Basis Sets	B1	A1	A2	D1	D2	D3
6-31G	4.1302	66.783	43.4	90.2	-178.8	-179.2
6-31G*	4.3658	69.907	42.9	91.5	-178.0	-176.8
6-31+G	4.0152	68.405	44.3	91.1	-179.5	-180.5
6-31+G*	4.4023	69.790	43.1	91.9	-177.1	-177.5
6-311G	4.2540	68.070	42.4	91.3	-178.3	-177.8
6-311G*	4.2814	68.156	43.5	90.7	-178.8	-178.1
6-311G (df,p)	4.3330	68.815	43.3	91.2	-178.2	-176.8

Table 5.9 HF, DFT//HF, and BSSE corrected DFT//HF binding energies E_b (kJ/mol). Vertical distance between 2,4-DNT and Siloxane Surface (Å).

Basis Sets	E_b (HF)	E_b (DFT//HF)	E_b /BSSE (DFT//HF)	VD
6-31G	51	46	26	3.5
6-31G*	33	32(32)[a]	17(18)	3.6
6-311G*	37	36	19	3.5
6-311G (df,p)	34	33	17	3.5

[a]B3LYP/6-31G* values in parentheses.

The BSSE binding energies computed with the basis sets augmented by polarization functions, i.e. 6-31G*, 6-311G* and 6-311G (df,p) basis sets, are ~9 kJ/mol smaller than that calculated with the simple basis sets. This indicates that the polarization functions describe more accurate the electron distribution. The E_b values in parenthesis correspond to the optimization of the interaction using DFT (B3LYP), at 6-31G* basis set, instead of the HF method. The values obtained using the DFT/6-31G* were similar to the ones calculated with the DFT//HF/6-31G* method. Therefore, the DFT//HF method has a good precision to reach the approximation adopted for the DFT method with lower computational cost.

Not all ab initio methods are suitable for supermolecule calculation. As we discuss before, the intermolecular interaction energy is a contribution of electrostatic, polarization, dispersion, and exchange interaction energy. The Hartree-Fock method does not include the dispersion interaction energy, which involves electron correlation between electrons on different molecules. DFT is a good option for intermolecular energy because it includes naturally exchange-correlation functionals, equally than the MP2 method. In the limit of large intermolecular distances, interaction energies can be approximated by perturbation theory[19,42]. MP2 is a perturbation method that includes the dispersion energy calculation, which arises from the mutual correlation of electrons which belong to different molecules[21]. Furthermore, in order to evaluate the contribution of the dispersion energy using the MP2 method we use a reduced molecular model of the surface to minimize the computational cost.

This model correspond to a single tetrahedra and cannot be considered as an adequate model of the surface because is too small. In Figure 5.5 we can see the interaction between 2,4-DNT with the tetrahedra. For this interaction we used the DFT//MP2 and DFT//HF methods at several basis sets that included polarization and diffuse functions.

Table 5.10 present the BSSE corrected binding energies of the DNT and tetrahedra interaction using the MP2 and DFT methods and the optimum VD between the molecules. It can be observed that the DFT method underestimates the E_b, in comparison with the MP2 method. This is due to the fact that DFT does not include the dispersion energy. Disappointingly, current DFT methods fail completely for the evaluation of dispersion energy. The reason is that none of the existing correlation functionals can describe the dispersion interaction[22,23]. This suggests that the DFT method is inadequate to describe the E_b of the DNT in the surface. The dispersion energy contribution can be calculated as followed:

$$DE_b = E_b\,(MP2) - E_b\,(DFT) \qquad (5)$$

Second-order Moller Plesset theory is the most economical post HF method. Surprisingly, this method gives very accurate intermolecular correlation energies. This is due to mutual compensation of neglected higher-order contributions[24].

Table 5.10 BSSE corrected MP2//HF and DFT//HF binding energies (kJ/mol), E_b(MP2) and E_b(DFT) respectively. Contributions of dispersion interactions to the binding energy DE_b, and the vertical distance (Å).

Basis Set	E_b/BSSE (MP2//HF)	E_b/BSSE (DFT//HF)	DE_b	VD
6-31G	13	10	3	3.5
6-31+G	17	12	5	3.4
6-31G*	12	6	6	3.6
6-31+G*	17	8	9	3.7
6-311G*	13	7	6	3.6
6-311+G*	17	8	9	3.6

In Table 5.10 the higher contribution of the dispersion energy was seen when we calculated the E_b using the basis sets that included the polarization and diffuse functions (which symbols are * and +, respectively). Computational limitations require finding a good balance between optimum solutions for problems between the size of the system and the level of computation[37]. In base of this we conclude that the best basis set that represent the dispersion contribution was 6-31+G* because produce a similar value than the largest basis set 6-311+G* with lower computational cost.

Finally we calculated the E_b using the BSSE corrected MP2 and DFT methods and determined the dispersion energy contribution presented in Table 5.11 for the DNT and siloxane surface interaction (Figure 5.13b). This table present that using the basis set 6-31+G* we can obtained the higher dispersion energy contribution to the E_b total between DNT and the siloxane surface. This binding energy corresponds to 42 kJ/mol[43] at a ~3.7 Å of distance between these molecules. This E_b is in excellent accordance with the experimental data (ΔH ~40 kJ/mol)[32].

Table 5.11 BSSE corrected MP2//HF and DFT//HF binding energies (kJ/mol), E_b(MP2) and E_b(DFT) respectively. Contributions of dispersion interactions to the binding energy DE_b, and the vertical distance (Å).

Basis Set	E_b/BSSE (MP2//HF)	E_b/BSSE (DFT//HF)	DE_b	VD
6-31G	35	26	9	3.5
6-31+G	42	27	15	3.7
6-31G*	35	17	18	3.6
6-31+G*	42	19	23	3.7

V.4 Solvation effect on the DNT spectroscopic signatures

V.4.1 Structural parameters analysis

There is a high possibility that the explosive molecules make contact with water from rain, for example when the buried landmines leak their content. Consequently, it is important to analyze the water effect on the explosives to determine change in the DNT chemical signature.

This analysis corresponds to a theoretical calculation of the solvation effect on the DNT molecular properties, using water as solvent. Data of bond lengths, bond angles, and torsion angles of DNT molecule in gas phase and solvated are show in Tables 5.12, 5.13 and 5.14. This study tries to determine if there is some change in the DNT molecular geometry when it is in the presence of a solvent. For this analysis we use water as solvent which dielectric constant is $\varepsilon = 78.39$, and the calculations were performed using the Onsager and PCM solvation model. A molecular volume calculation is necessary for the Onsager model, and this result in a cavity radius of 4.48 Å. Also, we calculate the vibrational frequencies as other alternative to measure the solvent effect in the DNT molecule.

Table 5.12 B3LYP/6-311+G** optimized calculated bond length of DNT and DNT solvated with water using the Onsager and PCM models.

Bonds (Å)	B3LYP/6-311+G**				
	Gas Phase	**Onsager**	**PCM**	$\Delta_{Onsager}$	Δ_{PCM}
C(5)-C(6)	1.3878	1.3876	1.3874	-0.0002	-0.0004
C(4)-C(5)	1.3904	1.3921	1.3925	0.0017	0.0021
C(3)-C(4)	1.3844	1.3840	1.3854	-0.0004	0.0010
C(2)-C(3)	1.3895	1.3890	1.3892	-0.0005	-0.0003
C(1)-C(6)	1.4033	1.4053	1.4032	0.0020	-0.0001
C(1)-C(16)	1.5056	1.5043	1.5041	-0.0013	-0.0015
<CC>	**1.4102**	**1.4104**	**1.4103**	**-**	**-**
H(8)-C(5)	1.0814	1.0816	1.0853	0.0002	0.0039
H(9)-C(6)	1.0835	1.0833	1.0872	-0.0002	0.0037
H(7)-C(3)	1.0804	1.0793	1.0840	-0.0011	0.0036
H(19)-C(16)	1.0907	1.0899	1.0904	-0.0008	-0.0003
H(17)-C(16)	1.0912	1.0911	1.0918	-0.0001	0.0006
H(18)-C(16)	1.0919	1.0923	1.0929	0.0004	0.0010
<HC>	**1.0865**	**1.0863**	**1.0886**	**-**	**-**
C(2)-N(10)	1.4825	1.4819	1.4745	-0.0006	-0.0080
C(4)-N(13)	1.4798	1.4758	1.4696	-0.0040	-0.0102
<CN>	**1.4811**	**1.4789**	**1.4721**	**-**	**-**
N(10)-O(11)	1.2225	1.2268	1.2266	0.0043	0.0041
N(10)-O(12)	1.2240	1.2216	1.2252	-0.0024	0.0012
N(13)-O(15)	1.2237	1.2277	1.2264	0.0040	0.0027
N(13)-O(14)	1.2225	1.2275	1.2267	0.0050	0.0042
<NO>	**1.2232**	**1.2259**	**1.2262**	-	-

Table 5.13 B3LYP/6-311+G** optimized calculated bond angles of DNT and DNT solvated with water using the Onsager and PCM models.

Angles (deg.)	B3LYP/6-311+G**				
	Gas Phase	**Onsager**	**PCM**	$\Delta_{Onsager}$	Δ_{PCM}
C(4)-C(5)-C(6)	118.7	118.7	118.7	0.0	0.0
C(3)-C(4)-C(5)	121.5	121.4	121.6	-0.1	0.1
C(2)-C(3)-C(4)	118.2	118.4	117.9	0.2	-0.2
C(1)-C(6)-C(5)	122.5	122.6	122.4	0.1	-0.1
C(16)-C(1)-C(6)	119.1	119.1	119.0	-0.1	-0.1
<CCC>	**120.0**	**120.0**	**119.9**		
H(8)-C(5)-C(6)	121.6	121.3	120.7	-0.3	-0.8
H(9)-C(6)-C(5)	119.1	119.0	118.9	-0.1	-0.2
H(7)-C(3)-C(4)	121.0	121.0	121.3	0.0	0.3
H(19)-C(16)-C(1)	109.7	109.9	109.6	0.2	-0.2
H(17)-C(16)-C(1)	112.0	112.1	112.0	0.1	0.0
H(18)-C(16)-C(1)	110.9	110.8	110.7	-0.1	-0.1
<HCC>	**115.7**	**115.7**	**115.5**		
N(10)-C(1)-C(2)	121.3	121.7	121.2	0.4	-0.1
N(13)-C(3)-C(4)	119.0	118.7	118.8	-0.3	-0.2
<NCC>	**120.2**	**120.2**	**120.0**		
O(11)-N(10)-C(2)	117.7	117.3	117.8	-0.4	0.1
O(12)-N(10)-C(2)	119.5	118.0	118.2	-1.5	-1.2
O(15)-N(13)-C(4)	117.3	117.7	117.0	0.4	-0.3
O(14)-N(13)-C(4)	117.6	117.7	117.9	0.1	0.4
<ONC>	**118.0**	**117.7**	**118.2**		

Table 5.14 B3LYP/6-311+G** optimized calculated dihedral angles of DNT and DNT solvated with water using the Onsager and PCM models.

Dihed. Angles (deg.)	B3LYP/6-311+G**				
	Gas Phase	Onsager	PCM	$\Delta_{Onsager}$	Δ_{PCM}
C(3)-C(4)-C(5)-C(6)	0.2	0.1	0.1	-0.1	0.0
C(2)-C(3)-C(4)-C(5)	-1.2	-1.0	-1.1	0.2	0.0
C(1)-C(6)-C(5)-C(4)	1.0	1.0	1.0	-0.1	0.0
C(16)-C(1)-C(6)-C(5)	-180.0	-180.0	-179.8	0.0	0.2
H(8)-C(5)-C(6)-C(1)	-179.3	-179.3	-179.3	0.0	0.0
H(9)-C(6)-C(5)-C(4)	-179.0	-179.1	-178.9	-0.1	0.1
H(7)-C(3)-C(4)-C(5)	178.8	178.9	179.6	0.1	0.8
H(19)-C(16)-C(1)-C(6)	12.2	12.4	13.3	0.1	1.1
H(17)-C(16)-C(1)-C(6)	133.2	133.5	134.3	0.3	1.1
H(18)-C(16)-C(1)-C(6)	-108.0	-107.7	-106.6	0.3	1.5
N(10)-C(2)-C(3)-C(4)	-179.0	-178.8	-179.0	0.2	0.0
N(13)-C(4)-C(5)-C(6)	179.9	179.9	180.0	0.0	0.1
O(11)-N(10)-C(2)-C(3)	-29.0	-26.8	-30.2	2.1	-1.2
O(12)-N(10)-C(2)-C(3)	150.3	152.1	149.2	1.9	-1.1
O(15)-N(13)-C(4)-C(5)	-0.4	-0.5	0.2	-0.1	0.6
O(14)-N(13)-C(4)-C(5)	179.6	179.5	180.2	-0.1	0.7

The optimized C-C bond lengths did not vary significantly with respect to gas phase data. Around ±0.0017 Å for the Onsager model and ±0.0021 Å for the PCM model. The C-H bonds changes using the Onsager model were of ±0.0011 Å, whereas for PCM model was from 0.0036 to 0.0039 Å for the methyl C-H bonds and from -0.0003 to 0.0010 Å for the ring C-H bonds. The C-N bonds are smaller when the DNT molecule is solvated.

The N(10)-O(12) bond (Figure 5.14) correspond to the nitro group in position 2 (the most close to the methyl group), where occur several intramolecular bonds which in gas phase has a long of 1.2240 Å . This bond is longer than the N(10)-O(11) (1.2225 Å) that is located, although in the 2-NO_2 group, distant of the methyl group. Meanwhile in the optimized geometry of the DNT solvated with both methods, we obtained the inverse situation. The solvation calculations made the N(10)-O(12) bonds shorter than N(10)-O(11) bonds, making the intramolecular interaction weaker. In Figure 5.14 we can compare the intramolecular interactions present in the DNT molecular structure when it is in gas-phase and solvated using the PCM model. The comparison with the Onsager model is not effectuated because does not exhibit significant changes.

The solvated bond angles calculated with Onsager and PCM solvation models do not varied significantly. Whereas the torsion angles are the most critical because are very sensitive to the calculation method used and the presence of substituents.

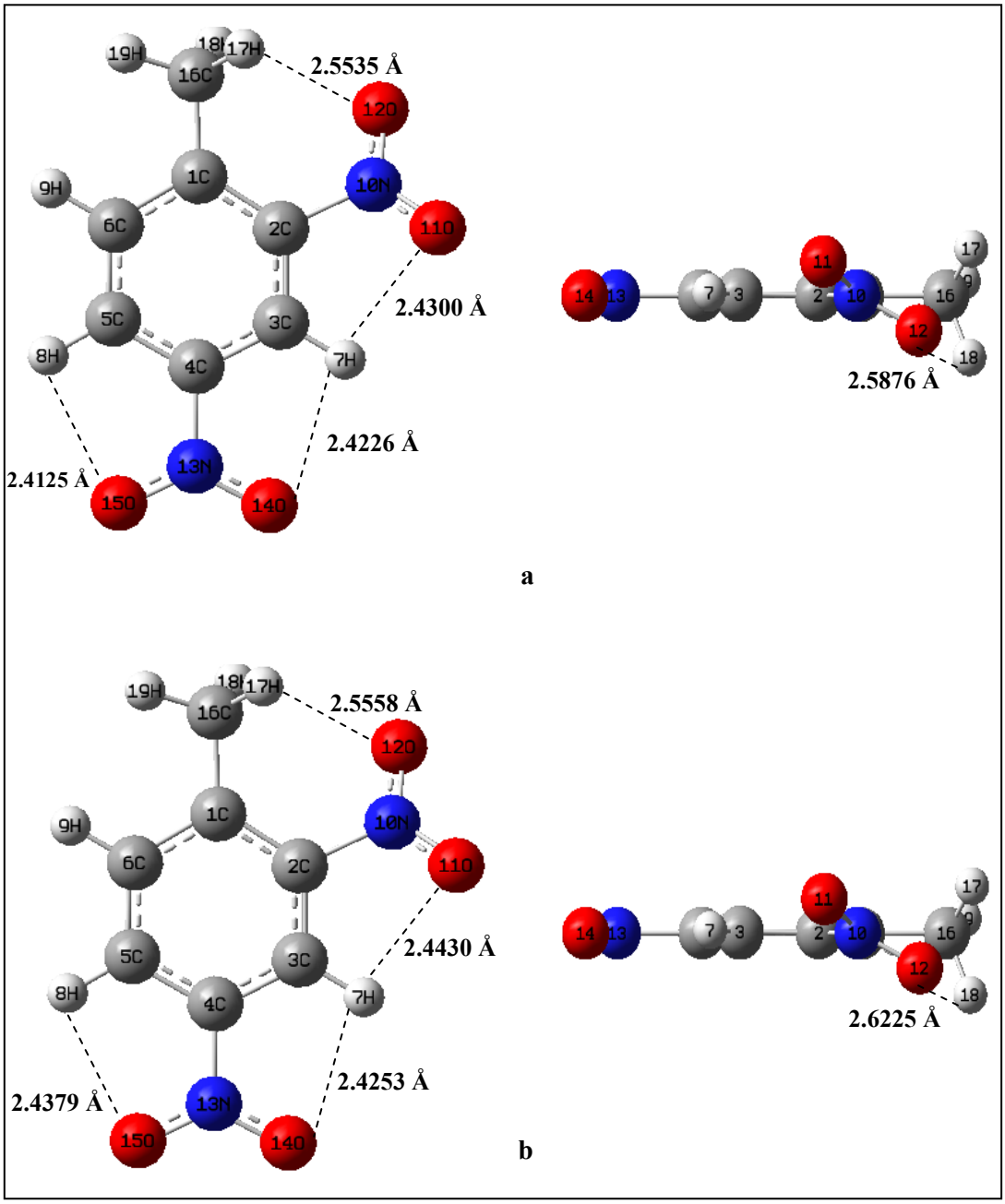

Figure 5.14. B3LYP/6-311+G** Optimized molecular structure of DNT in (a) gas-phase and (b) solvated with PCM model. Left: Top view and right: side view.

V.4.2 Solvation effect in the stability of the DNT molecule

The absolute energies from the B3LYP/6-311+G** calculations for the DNT molecule in gas phase and with the effects of solvation are shown in Table 5.15. The energies obtained with the solvation models are more negative than in the gas phase. We can see that the DNT molecule is most stable solvated than in gas phase. The PCM model simulate a much more realistic shape than the Onsager model, whose charge distribution of solute is represented by a simple dipole and is embedded in a typically spherical cavity and interacts with the solvent.

Therefore, the higher energy differences between the DNT molecule solvated and in gas phase are observed with the PCM model which value differs for about -11.1 kcal/mol. On the other hand the Onsager model estimated an energy of these interactions or solvent effect of -2.8 kcal/mol. This poor solvent effect obtained with the Onsager model possibly is because this method have to be use with solutes of approximately spherical shape and those whose interactions with the medium may be justifiably represented by dipole-dipole ones. Whereas for PCM allow us to study molecules with non-spherical shape and charge distribution. In this case a cavity has a much more realistic shape and is constructed of certain number of interlocking spheres.

Table 5.15 The absolute (a.u.) energies of DNT at B3LYP/6-311+G**, Onsager and PCM optimization level. Delta energies between DNT being solvated and in gas phase.

B3LYP/ 6-311+G**	Gas-phase	PCM	Onsager	ΔE_{PCM}		$\Delta E_{Onsager}$	
				hartrees	kcal/mol	hartrees	kcal/mol
DNT (hartrees)	-680.7572	-680.7749	-680.7617	-0.0177	-11.1	-0.0045	-2.8

V.4.3 Vibrational frequencies analysis of the solvation effect on DNT

In general the spectrum of DNT in each solvation models looks similar, showing the same characteristic bands. These band assignments of the fundamental frequencies have been made based on the gas phase spectrum.

In case of the Onsager model it considers a single molecule surrounded by a uniform interacting field representing the solvent. It does not take into account any interaction of a solute with other solute molecules, which could be present if a concentrated solution is considered. In this model the molecular dipole induce a dipole in the medium, and the electric field applied to the solute by the solvent dipole interact in turn with the molecular dipole to lead to net stabilization and an associated frequency shift. In the calculations, the electrostatic solvent effect describes the coupling between the molecular dipole and the reaction field (solvent). Meanwhile, PCM model describe of solute-solvent interactions, providing us with a means of taking into account a mutual polarisation of solute and solvent in a self-consistent way.

We can observe those shifts graphically in the figures below. Figures 5.15, 5.16 and 5.17 show the spectra of DNT in gas-phase, and solvated using the PCM and Onsager models in ranges of 650-1200, 1300-1700, 2950-3300 cm^{-1}.

In Figure 5.15 we can observe how all the DNT features bands are reproduce very well in all spectra. Also is notable the slight blue shift tendency which occur mainly in the order of PCM < Onsager model spectra in comparison with the gas-phase spectrum. Also the peaks intensities increase in the order of Onsager < PCM spectrum.

The NO_2 symmetric and asymmetric bands at 1300-1700 cm^{-1} range are shown in Figure 5.16, even the bands that correspond to the ring and 2-NO_2 group coupled. This range present a remarkable blue shift that follow the tendency of PCM < Onsager frequencies. A new peak appears at 1346 cm^{-1} and at 1341 cm^{-1} on the DNT spectra solvated with Onsager and PCM models respectively. These peaks are attributed to a vibration related with the symmetric NO_2 stretching. In the PCM model this new peak decrease the intensity of the 1351 cm^{-1} symmetric band, but the peaks of the asymmetric vibrations are more intense than respective bands in the Onsager spectrum.

The characteristics vibrational frequencies for the DNT molecule, the symmetric and asymmetric NO_2 bands, are shown in Table 5.16. It is evident that the frequencies in the DNT solvated are shifted, which indicates an effect of the solvent on the absorption band. In Table 5.17 is summarized the frequency shifts obtained for the main vibrational bands (of the NO_2 group) with respect to the gas phase. In Appendix 5.3 is showing all the vibrational frequencies of DNT in gas phase and DNT solvated with Onsager and PCM models.

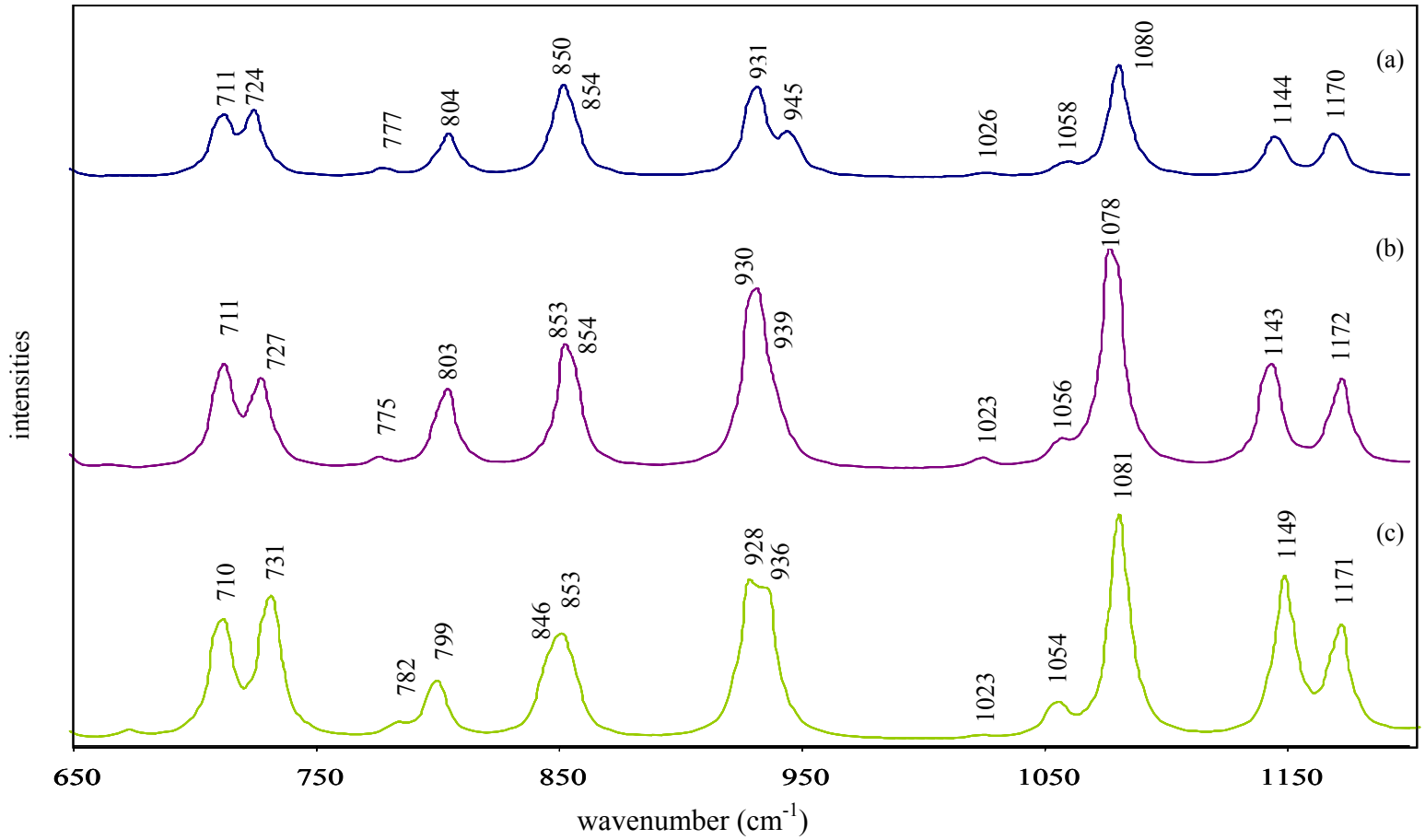

Figure 5.15 B3LYP/6-311+G** IR spectra of DNT in gas phase and solvated: (a) gas-phase (b) Onsager model (c) PCM model at 650-1200 cm^{-1}

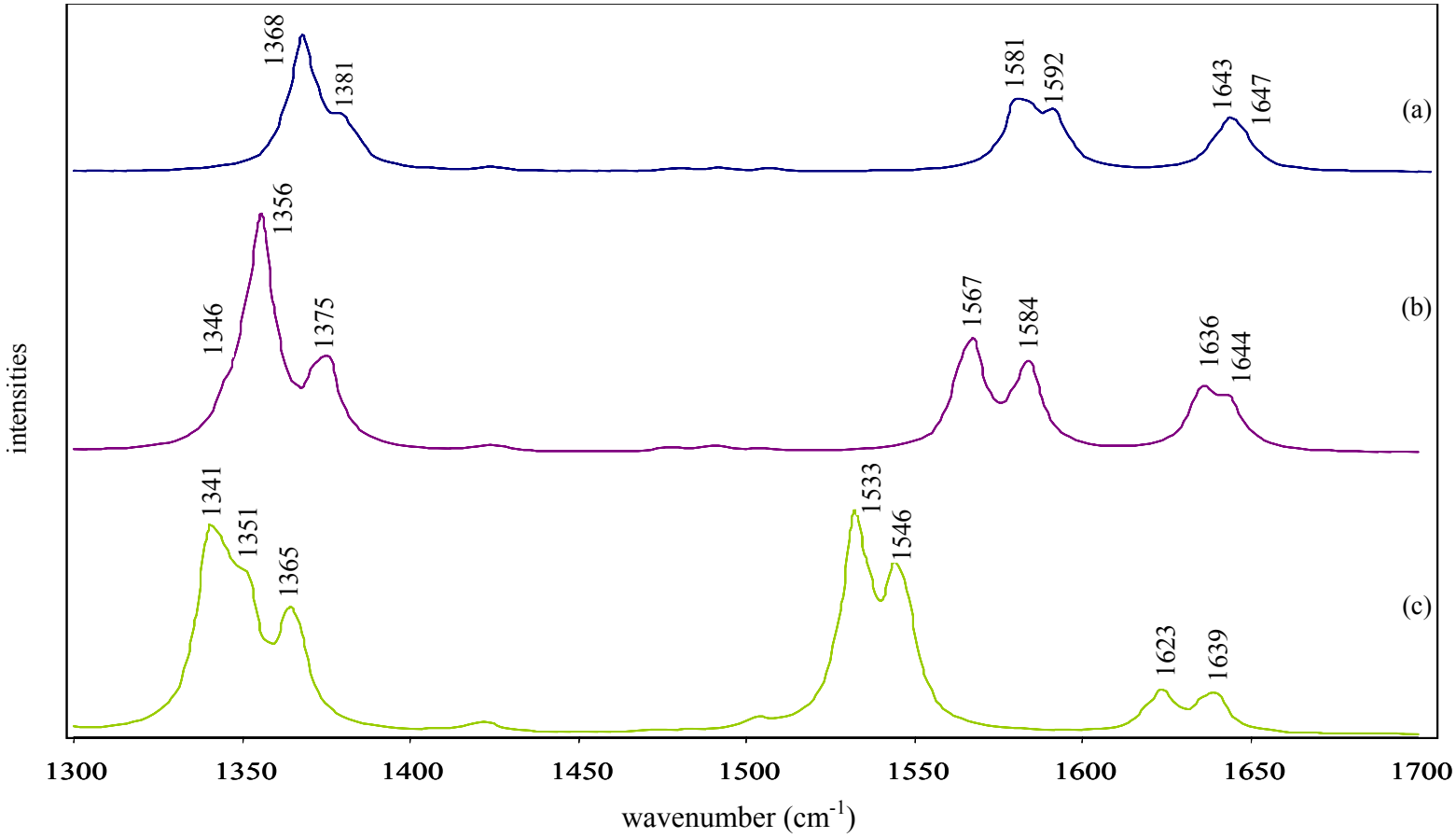

Figure 5.16 B3LYP/6-311+G** IR spectra of DNT in gas phase and in solution: (a) gas-phase (b) Onsager (c) PCM at 1300-1700cm^{-1}

Table 5.16 B3LYP/6-311+G** calculation of the NO_2 vibrational frequencies of DNT in gas-phase and in solution. The latter using the Onsager and the PCM solvation models.

Medium	Model	vibrational frequencies (cm^{-1})			
		υ_{35}	υ_{36}	υ_{42}	υ_{43}
gas phase	Theoretical	1368	1381	1581	1592
water	Onsager	1356	1375	1567	1584
	PCM	1351	1365	1533	1546

Table 5.17 B3LYP/6-311+G** calculation of the NO_2 vibrational frequencies shifts of DNT in solution compare with the DNT in gas-phase.

Medium	Model	$\Delta\upsilon$ (cm^{-1})			
		υ_{35}	υ_{36}	υ_{42}	υ_{43}
water	Onsager	-12	-6	-14	-8
	PCM	-27	-16	-48	-46

In Figure 5.17 is showing the C-H region from 2950 to 3300 cm^{-1}. The spectrum of DNT solvated with the Onsager model present red shifts in the methyl C-H of 2 cm^{-1} (3052 cm^{-1}) and of 8 cm^{-1} (3132 cm^{-1}), whereas on the ring C-H are of 6 cm^{-1} (3192 cm^{-1}) and of 9 cm^{-1}(3247 cm^{-1}). The other two peaks at 3109 cm^{-1} and at 3223 cm^{-1} which represent the methyl and ring C-H vibrations, respectively, does not exhibit any shift. The intensities of the DNT peaks in gas-phase and solvated with Onsager model have similar intensities.

In the other hand, the spectrum of DNT solvated with the PCM model presents the same blue shift tendency. The methyl C-H vibrations shifts are of -10 cm^{1} (3040 cm^{1}), -11 cm^{1} (3098 cm^{1}) and -7 cm^{1} (3117 cm^{1}). The ring C-H vibrations exhibit an abrupt blue shifts of -77 cm^{1} (3117 cm^{1}) and -89 cm^{1} (3117 cm^{1}). The frequencies decreases are related to the increase in the bond lengths. In Table 5.12 we can observe an increase from 0.0036 to 0.0039 Å in the ring C-H bonds. One of the ring C-H peaks was overlap by the others two peaks.

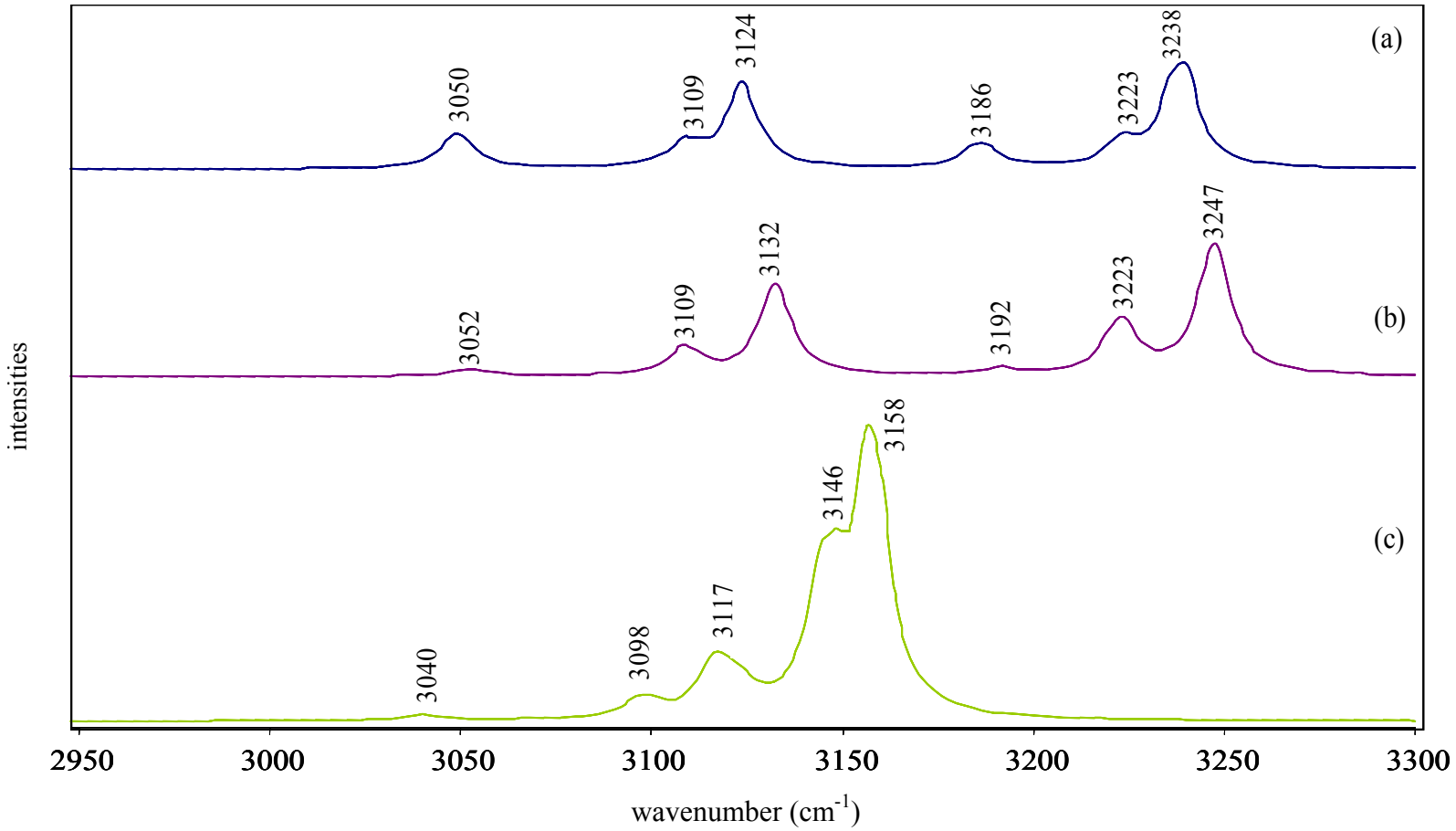

Figure 5.17 B3LYP/6-311+G** IR spectra of DNT in gas phase and in solution: (a) gas-phase (b) Onsager (c) PCM at 2950-3300 cm^{-1}

The calculated frequency shifts of DNT solvated, compared with those obtained in gas phase reflect the influence of the dielectric constant of the solvent on the absorption frequencies. According to the theoretical calculations, most of the frequency shifts are expected to be negative as a result of the interaction of the molecular dipole and the dielectric field of the solvent, in which the attractive force of the intermolecular potential is dominant[29].

VII. CONCLUSIONS

The most stable conformation of the 2,4-DNT has been calculated using DFT procedures and a variety of basis sets from the Gaussian system of programs. 2,4-DNT lowest-energy conformation has C_1 symmetry and was obtained with the 6-311+G** basis set. The calculations yielded the molecular symmetry, structural parameters, and vibrational spectra for the conformer. The genuine energy minimum structure was found. This was verified by the vibrational frequency calculations since no negative frequencies were found.

The results indicates that DFT is a very good method to study DNT since the calculated internal coordinates (bond lengths, and bond angles), and the vibrational frequencies are in good agreement with the experimental values. IR spectra of DNT have been measured and compared with the simulated spectra. The ranges of 600-1200 cm^{-1} and 1300-1700 cm^{-1}, have a good tendency of the bands. Whereas the theoretical range of 2950-3300 cm^{-1} do not reproduce well the experimental spectrum. The calculated symmetric and asymmetric nitro group stretching frequencies are a good spectroscopic signature for DNT due to the large IR intensities. The main changes in the spectroscopic signature of DNT with respect to the DNT-clay mineral or siloxane surface are in the red shifts of the NO_2 symmetrical and asymmetrical vibrational stretchings. This indicated that exist an interaction between the complexes.

The noncovalent intermolecular interaction of the DNT-siloxane complex was calculated to determine the binding energy (E_b) between the DNT molecule and siloxane surface. There is a weak E_b since the DNT structure is non-coplanar with respect to the surface. The MP2//HF binding energy at 6-31+G* basis set (42 kJ/mol) is in excellent accordance with the experimental data (ΔH ~40 kJ/mol). We have found that this binding energy is described more accurately by the polarized and diffused basis functions. This is due to the dispersion energy contribution that in this case is 23 kJ/mol. The interaction between the DNT and the siloxane surface occurred at ~3.7 Å of distance.

In the solvation analysis we found that the explosive molecule has a lower energy solvated using with the PCM model. The energy differences between the DNT molecule in gas phase and solvated with the PCM model is -11.1 kcal/mol, meanwhile for the Onsager model solvent effect the difference is -2.8 kcal/mol. The fact that the Onsager is not the best method could be possible associate to the fact that this model is mainly used for molecules with spherical shape. The O-N intramolecular interactions, between the methyl and 2-NO_2, may disappear using the PCM model because the distance is higher than 2.6 Å which is larger than the sum of vdW radii. This could be possible due the fact that the PCM form a cavity surface (vdW surface) which size is the sum of the heavy atom (except H's) spheres. The solvent effect occurs in the vdW surface that includes only the heavy atoms. Therefore, the H atoms are free to stretch their bonds. The DNT spectrum solvated with the PCM model in the region of the

methyl and ring C-H vibrations present a different behavior in comparison with the DNT in gas-phase spectrum. The larger blue shift that present the ring C-H bands correspond to the increase of bond lengths.

Theoretical calculations will play a central role in the proposed study of surface explosives interactions. This information will be critical to the development of a new family of sensors for landmine explosive detection.

VII. FUTURE WORKS

- ❖ Perform an x-ray study in order to obtain the crystallographic data of 2,4-DNT to compare with theoretical structural parameters.

- ❖ Perform experimental interactions between DNT and other clay minerals with expandable capacity (e.g. montmorillonite).

- ❖ Perform theoretical interactions between DNT with:
  - siloxane sheet
  - another molecule of DNT and siloxane sheet
  - the hydroxyl surface of the kaolinite

- ❖ Perform experimental solvation analysis to the DNT molecule for comparison purpose.

- ❖ In base of the experimental data of solvation, perform theoretical calculation with others solvation models to determine which one give the best reproduction of the experimental spectra.

VIII. REFERENCES

1. S. B. Haderlein, K. W. Weissmahr and R. P. Schwarzenbach, "Specific Adsorption of Nitroaromatic Explosives and Pesticides to Clay Minerals", *Environ. Sci. Technol*., **30**, 1996, 612-622.

2. D. R. Hartter, *In toxicity of Nitroaromatic Compounds*, 1-13, Hemisphere, Washington, DC, 1985.

3. D. H. Rosenblatt, E. P. Burrows, W. R. Mitchell, D. L. Parmer, *In The Handbook of Environmental Chemistry-Anthropogenic Compounds*, 195-237, Springer Verlag, Berlin, 1991.

4. A. Crockett, T. Jenkins, H. Craig, and W. Sisk, *Overview of on-Site Analytical methods for Explosives in Soil*, US Army Corps of Engineers, Cold Regions Research & Engineering Laboratory, Special report 98-4, 1998.

5. J. M. Phelan and S. W. Webb, Sandia National laboratory Report SAND2002-0909, Albuquerque NM, and Livermore, CA , May 2002.

6. J. Yinon, *Toxicity and Metabolism of Explosives*, CRC Press, Boca Raton, FL 1990.

7. M.J. Frisch, G.W. Trucks, H.B. Schlegel, G.E. Scuseria, M.A. Robb, J.R. Cheeseman, V.G. Zakrzewski, J.A. Montgomery, Jr., R.E. Stratmann, J.C. Burant, S. Dapprich, J.M. Millam, A.D. Daniels, K.N. Kudin, M.C. Strain, O. Farkas, J. Tomasi, V. Barone, M. Cossi, R. Cammi, B. Mennucci, C. Pomelli, C. Adamo, S. Clifford, J. Ochterski, G.A. Petersson, P.Y. Ayala, Q. Cui, K. Morokuma, D.K. Malick, A.D. Rabuck, K. Raghavachari, J.B. Foresman, J. Cioslowski, J.V. Ortiz, B.B. Stefanov, G. Liu, A. Liashenko, P. Piskorz, I. Komaromi, R. Gomperts, R.L. Martin, D.J. Fox, T. Keith, M.A. Al-Laham, C.Y. Peng, A. Nanayakkara, C. Gonzalez, M. Challacombe, P.M.W. Gill, B. Johnson, W. Chen, M.W. Wong, J.L. Andres, C. Gonzalez, M. Head-Gordon, E.S. Replogle, and J.A. Pople, Gaussian 03, Revision A.3, Gaussian, Inc., Pittsburgh PA, 2003.

8. Web site: http://www.speclab.com/compound/ - (Material Safety Data Sheet - MSDS).

9. D.C. Leggett, T.F. Jenkins, and R.P. Murrmann, *Composition of Vapors Evolved from Military TNT as Influenced by Temperature Solid Composition, Age, and Source*, U.S. Army Engineer Research and Development Center, Cold Regions Research and Engineering Laboratory, Special Report 77-16, 1977.

10. E. Besoain. Mineralogía de Arcillas de Suelos, Instituto Interamericano de Cooperación para la Agricultura (IICA). San José, Costa Rica, 1985.

11. B.L. Allen and B.F. Hajek, *Mineral occurrence in soil environments*. J.B. Dixon and S.B. Weed (ed.), Minerals in soil environments 2nd ed., SSSA Book Ser. 1. SSSA, Madison, WI., 199-278,1989.

12. S.W. Bailey, *Crystal structures of clay minerals and their x-ray identification,* G.W. Brindley and G. Brown (ed.), Mineralogical Society, London, UK.,1-123,1980.

13. S. Fiore, F.J. Huertas, F. Huertas, and J. Linares, "Morphology of kaolinite crystals synthesized under hydrothermal conditions", Clays Clay Miner., 43:353-360, 1995.

14. J. B. Foresman and A. Frisch, *Exploring Chemistry with Electronic Structure Methods,* Chapter 1, Gaussian, Inc., Pittsburg, PA, 1996.

15. D.C. Young, *COMPUTATIONAL CHEMISTRY: A practical guide for applying techniques to real-world problems*, Wiley-Interscience, John Wiley & Sons, Inc., N.Y., 2001.

16. F. Jensen, *Introduction to Computational Chemistry,* John Wiley & Sons, Inc. N.Y., 1999.

17. H. dorsett and A. White, Overview of molecular modelling and ab initio molecular orbital methods suitable for use with energetic materials. DSTO, 1-35, 2000.

18. Web site: http://chemviz.ncsa.uiuc.edu/content/lab-s-basis.html

19. B. Jezionki, W. Kolos. *Molecular Interactions*. Eds. Wiley, New York, 3, 1982.

20. B. Jeziorski; R. Moszynski; K. Szalewicz, "Perturbation theory approach to intermolecular potential energy surfaces of van der Waals complexes", *Chem. Rev.*, **94**, 1994,1887-1930.

21. Y. Ma, "Determination of Noncovalent Intermolecular Interaction Energy from Electron Densities", Dissertation, University New Orleans, May 2004.

22. P. Hobza, J. Sponer, T. Reschel, *J. Comput. Chem.*, **11**, 1995, 1315.

23. S. Kristian, P. Pulay., "Can (semi) local density functional theory account for the London dispersion forces?", *Chem. Phys. Lett.* **229**, 1994, 175-180.

24. P. Hobza and K. Muller-Dethlefs, "Noncovalent interactions: A challenge for experiment and theory", *Chem. Rev.* **100**, 2000, 143-167.

25. H. B. Jansen, P. Ross, *Chem. Phys. Lett*., **3**, 1969, 140.

26. B. Liu, A. D. McLean, "Accurate calculation of the attractive interaction of two ground state helium atoms", *J. Chem. Phys*., **59**, 1973, 4557.

27. S. F. Boys, F. Bernardi, "The calculation of small molecular interactions by the differences of separate total energies. Some procedures with reduced errors", *Mol Phys*, **19**, 1970, 553.

28. A. Szarecka, J. Rychlewski, U. Rychlewska, "Theoretical solvation models: ab initio of molecular aggregation", Computational Methods in Science and Technology, **4**,1998, 25-33.

29. D. L. Cedeno, J. Peng, D. Reynolds, N. Mina-Camilde and C. Manzanares. "Infrared absorptions and band widths of dilute solutions of CF3H in liquid Ar, N2, and Xe". *Molecular physics*, **96**, 1999, 1745-1755.

30. P. C. Chen, W. Lo, K.H. Hu, "Ab initio studies of the molecular structures of dinitrotoluenes", *Journal of Molecular Structure (Theochem)*, **389**, 1997, 91-96.

31. E. Balan, A. M. Saitta, F. Mauri and G. Calas, "First-principles modeling of the infrared spectrum of kaolinite", *American Mineralogist*, **86**, 2001, 1321-1330.

32. S. B. Haderlein and R.P. Schwarzenbach, "Adsorption of Substituted Nitrobenzenes and Nitrophenols to Mineral Surfaces", *Environ. Sci. Technol.*, **27**, 1993, 316-326.

33. A. Frisch, R. D. Dennington II, T. A. Keith, A. B. Nielsen and A. J. Holder, *Gauss View*, Gaussian Inc. Carnegie, PA 2003.

34. D.L. Bish, R. B. Von Dreele, "Rietveld refinement of non-hydrogen atomic positions in kaolinite", *Clays and Clay Miner*., **37**, 1989, 289-296.

35. D.L. Bish, "Rietveld refinement of the kaolinite structure at 1.5K", *Clays and Clay Miner*., **41**, 1993, 738-744.

36. A. Pelmenschikov and J. Leszczynski, "Adsorption of 1, 3, 5-Trinitrobenzene on the Siloxane Sites of Clay Minerals: Ab Initio Calculations of Molecular Models". *J. Phys. Chem. B*, **103,** 1999, 6886-6890.

37. J. Sauer, P. Ugliengo, E. Garrone, and V. Saunders, "Theoretical Study of van der Waals Complexes at Surface Site in Comparison with the Experiment", *Chem. Rev.,* **94**, 2095-2160, 1994.

38. A. Frisch, M.J. Frisch and G.W. Trucks, *Gaussian 03 User's Reference*, Gaussian, Inc.: Carnegie, PA, 2003.

39. Y. Colón, C. Ramos, L. Alzate, A. Santana, S. Hernández, M. Castro, J. Briano, M. Muñoz, and N. Mina, "Adsorption of RDX on Clay in Proceedings of the SPIE Vol. 5415 Detection and Remediation Technologies for Mines and Minelike Targets IX; edited by Russell S. Harmon, J. Thomas Broach, John H. Holloway,(SPIE, Bellingham, WA, 2004) 1419-1430.

40. C. Ramos, L. Alzate**,** Y. Colón, A. Santana, S. Hernández, M. Castro, J. Briano, and N. Mina, "Theoretical studies of the Molecular Structures of Dinitrotoluenes and their Interactions with Siloxane Surface of Clay Minerals", in Proceedings of the SPIE Vol. 5415 Detection and Remediation Technologies for Mines and Minelike Targets IX; edited by Russell S. Harmon, J. Thomas Broach, John H. Holloway,(SPIE, Bellingham, WA, 2004) 1377-1388.

41. W. Koch and M. C. Holthausen, A Chemist's Guide to Density Functional Theory, Ed. 2nd, Chapter 8, Wiley-VCH, Republic of Germany, 2001.

42. Chalasiski, G.; Gutowski, M., "Weak interactions between systems. Models for studying the nature of intermolecular forces and challenging problems for ab initio", *Chem. Rev.,* **88**, 943, 1988.

43. C. Ramos, L. Alzate**,** Y. Colón**,** S. Hernández, and N. Mina, "Computational Modeling of the Adsorption of 2,4-DNT on Clay", in Proceedings of the SPIE Detection and Remediation Technologies for Mines and Minelike Targets X; edited by Russell S. Harmon, J. Thomas Broach, John H. Holloway,(SPIE, Bellingham, WA, 2005) (in press).

IX. APPENDIX

Appendix 5.1 Z-matrix of the DNT molecular structure optimization using B3LYP/6-311g(d)

```
%mem= 800mb
%Chk=Dopt5of
# b3lyp/6-311g(d) opt=z-matrix

Optimization of the DNT molecular structure

0  1
 C
 C            1          B1
 C            2          B2    1          A1
 C            3          B3    2          A2    1          D1
 C            4          B4    3          A3    2          D2
 C            1          B5    2          A4    3          D3
 H            2          B6    1          A5    6          D4
 H            1          B7    2          A6    3          D5
 H            4          B8    3          A7    2          D6
 C            6          B9    1          A8    2          D7
 H           10         B10    6          A9    1          D8
 H           10         B11    6         A10    1          D9
 H           10         B12    6         A11    1         D10
 N            5         B13    4         A12    3         D11
 O           14         B14    5         A13    4         D12
 O           14         B15    5         A14    4         D13
 N            3         B16    2         A15    1         D14
 O           17         B17    3         A16    2         D15
 O           17         B18    3         A17    2         D16

  B1         1.389418
  B2         1.394589
  B3         1.385836
  B4         1.394470
  B5         1.409129
  B6         1.078462
  B7         1.080371
  B8         1.077159
  B9         1.506711
  B10        1.088846
  B11        1.089228
  B12        1.089748
  B13        1.471152
  B14        1.265613
  B15        1.266820
  B16        1.465927
  B17        1.266133
  B18        1.264617
```

A1	118.702064
A2	121.447253
A3	118.612657
A4	122.566715
A5	121.683787
A6	119.152107
A7	120.983329
A8	118.619694
A9	109.821483
A10	112.033189
A11	111.251716
A12	115.550119
A13	117.889136
A14	118.701969
A15	119.477064
A16	117.775687
A17	118.121985
D1	-0.024867
D2	-0.417686
D3	0.468515
D4	-179.694499
D5	-179.499014
D6	179.201392
D7	-179.970933
D8	7.939848
D9	129.063316
D10	-112.639451
D11	-179.773813
D12	-15.866020
D13	163.693992
D14	179.934009
D15	-0.444904
D16	179.558296

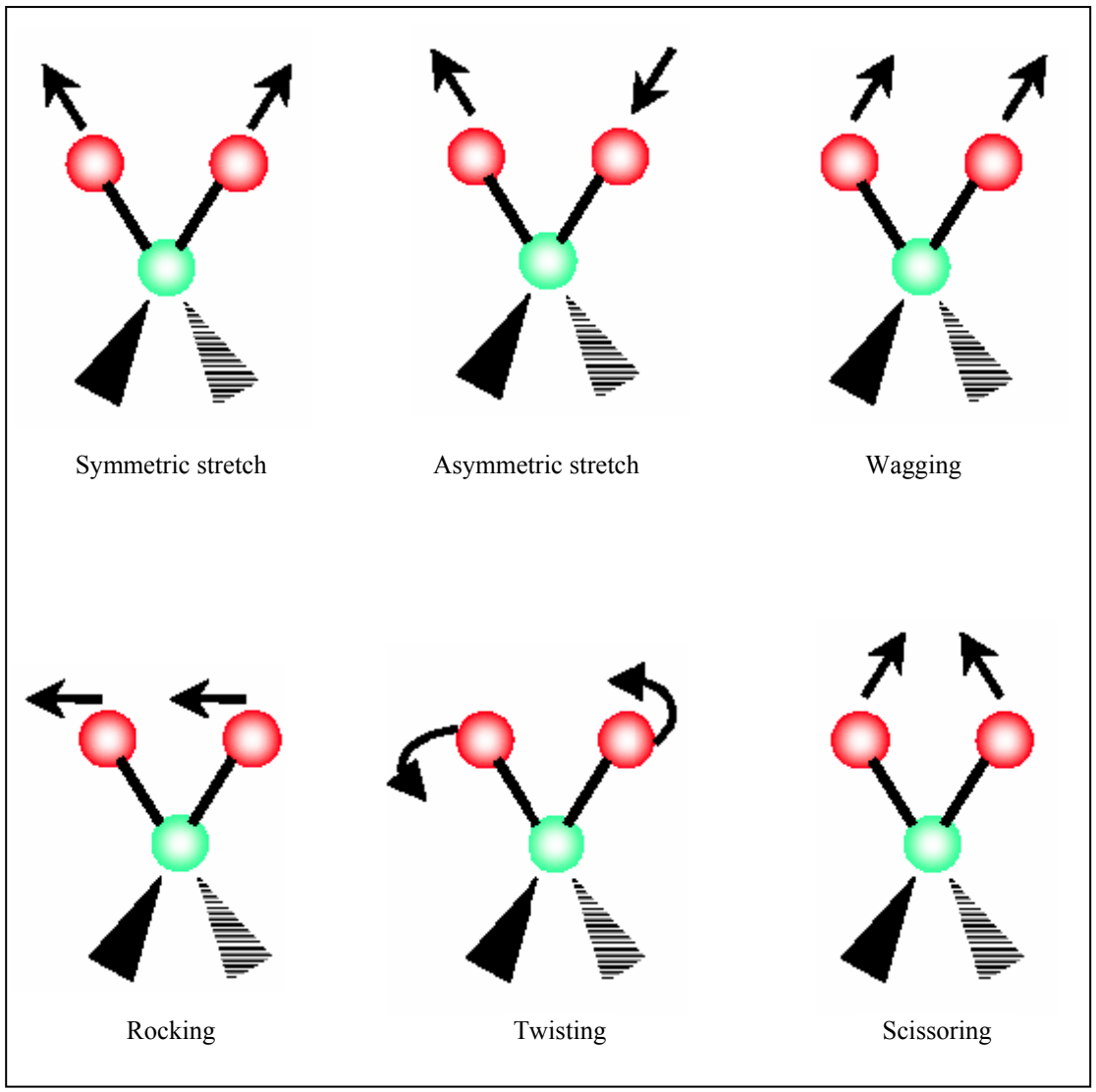

Appendix 5.2 Stretching and bending vibrational modes

Annex 5.3 B3LYP/6-311+G** IR frequencies and tentative assignments of DNT in gas-phase and solvated with water using the Onsager and PCM models.

ν	Theoretical							
	gas phase		PCM		Solvent shifts (Δ)	Onsager		Solvent shifts (Δ)
	Freq	IR Int	Freq	IR Int		Freq	IR Int	
1	43	0	50	1	7	45	0	2
2	49	0	55	1	6	48	1	-1
3	105	0	105	1	0	106	1	1
4	150	2	148	6	-2	152	2	2
5	164	4	168	11	4	165	6	1
6	186	1	189	2	3	182	2	-4
7	272	1	273	1	1	272	2	0
8	287	2	286	6	-1	288	3	1
9	343	1	344	3	1	345	2	2
10	351	1	353	1	2	352	3	1
11	394	0	395	0	1	394	1	0
12	436	1	428	3	-8	436	2	0
13	486	6	485	14	-1	488	9	2
14	532	3	530	12	-2	531	6	-1
15	575	0	580	1	5	574	0	-1
16	646	4	641	9	-5	646	7	0
17	668	0	672	3	4	666	1	-2
18	710	22	710	47	0	711	39	1
19	724	23	731	56	7	727	33	3
20	777	3	783	4	6	775	4	-2
21	804	16	799	23	-5	803	32	-1
22	849	18	846	27	-3	853	29	4
23	853	22	853	29	0	854	22	1
24	930	35	928	48	-2	930	73	0
25	945	14	936	44	-9	939	15	-6
26	998	0	998	0	0	1004	0	6
27	1026	1	1024	1	-2	1024	4	-2
28	1058	4	1054	12	-4	1056	7	-2
29	1080	43	1081	88	1	1078	93	-2
30	1144	15	1149	62	5	1143	42	-1
31	1169	17	1171	41	2	1172	33	3
32	1219	6	1221	28	2	1218	13	-1
33	1288	7	1292	40	4	1288	22	0
34	1347	0	1341	624	-6	1346	97	-1
35	1368	431	1350	390	-18	1356	749	-12
36	1381	126	1365	360	-15	1375	289	-5
37	1420	1	1410	4	-10	1419	3	-1
38	1425	12	1422	33	-3	1425	18	0
39	1479	8	1472	4	-7	1478	13	-1
40	1492	10	1485	3	-7	1491	19	-1
41	1507	8	1503	30	-4	1505	8	-2
42	1582	227	1533	674	-48	1567	373	-14
43	1592	161	1546	502	-46	1584	269	-8
44	1643	128	1623	132	-20	1636	175	-7
45	1647	81	1639	130	-8	1644	139	-3
46	3049	6	3040	1	-9	3052	1	3
47	3109	4	3098	5	-11	3109	5	0
48	3124	15	3117	12	-7	3133	16	9
49	3186	5	3123	6	-63	3192	1	6
50	3223	4	3146	39	-77	3223	10	0
51	3238	19	3158	73	-80	3247	23	9